NASA/TM–20220005181

A Damage Resistance Comparison of Wet-Wound IM7 and T1100 Carbon Fiber/Epoxy Cylinders

A.T. Nettles and A.M. Clark
Marshall Space Flight Center, Huntsville, Alabama

April 2022

NASA STI Program Report Series

The NASA STI Program collects, organizes, provides for archiving, and disseminates NASA's STI. The NASA STI program provides access to the NTRS Registered and its public interface, the NASA Technical Reports Server, thus providing one of the largest collections of aeronautical and space science STI in the world. Results are published in both non-NASA channels and by NASA in the NASA STI Report Series, which includes the following report types:

- TECHNICAL PUBLICATION. Reports of completed research or a major significant phase of research that present the results of NASA programs and include extensive data or theoretical analysis. Includes compilations of significant scientific and technical data and information deemed to be of continuing reference value. NASA's counterpart of peer-reviewed formal professional papers but has less stringent limitations on manuscript length and extent of graphic presentations.

- TECHNICAL MEMORANDUM. Scientific and technical findings that are preliminary or of specialized interest, e.g., quick release reports, working papers, and bibliographies that contain minimal annotation. Does not contain extensive analysis.

- CONTRACTOR REPORT. Scientific and technical findings by NASA-sponsored contractors and grantees.

- CONFERENCE PUBLICATION. Collected papers from scientific and technical conferences, symposia, seminars, or other meetings sponsored or cosponsored by NASA.

- SPECIAL PUBLICATION. Scientific, technical, or historical information from NASA programs, projects, and mission, often concerned with subjects having substantial public interest.

- TECHNICAL TRANSLATION. English-language translations of foreign scientific and technical material pertinent to NASA's mission.

Specialized services also include organizing and publishing research results, distributing specialized research announcements and feeds, providing information desk and personal search support, and enabling data exchange services.

For more information about the NASA STI program, see the following:

- Access the NASA STI program home page at http://www.sti.nasa.gov

- Help desk contact information:

https://www.sti.nasa.gov/sti-contact-form/ and select the "General" help request type.

NASA/TM–20220005181

A Damage Resistance Comparison of Wet-Wound IM7 and T1100 Carbon Fiber/Epoxy Cylinders

A.T. Nettles and A.M. Clark
Marshall Space Flight Center, Huntsville, Alabama

National Aeronautics and
Space Administration

Marshall Space Flight Center • Huntsville, Alabama 35812

April 2022

Acknowledgments

The authors wish to thank Phil Thompson and Andrew Martin for help in winding the test articles and Ian Johnston for securing funding for this task.

TRADEMARKS

Available from:

NASA STI Information Desk
Mail Stop 148
NASA Langley Research Center
Hampton, VA 23681–2199, USA
757–864–9658

This report is also available in electronic form at
<http://www.sti.nasa.gov>

TABLE OF CONTENTS

1. INTRODUCTION 1

2. MANUFACTURE OF TEST ARTICLES 2

   2.1 Overview 3
   2.2 Materials 4
   2.3 Dry Wind 6
   2.4 Cure Cycle 6
   2.5 IM7 Fiber Cylinder Manufacture 7
   2.6 T1100 Fiber Cylinder Manufacture 8

3. IMPACT TESTING 11

4. RESULTS OF IMPACT TESTING 19

5. STATIC INDENTATION TESTING 23

6. RESULTS OF STATIC INDENTATION TESTING 24

7. CONCLUSIONS 37

REFERENCES 38

LIST OF FIGURES

1. Schematic of cylinder lay-ups used for impact testing in this study 4

2. One of the two sand mandrels used to manufacture the cylinders used in this study 5

3. Dry winding to test filament winder settings before the actual wet winding is performed. Helical pattern shown on left and hoop pattern shown on right 6

4. Wet-wound IM7 fiber cylinder after addition of ninth layer 7

5. Wet-wound IM7 fiber cylinder being carried to (left) and placed into (right) the oven for curing 8

6. Undamaged cross sections in the hoop direction 9

7. Undamaged cross sections in the helical direction 10

8. Drop tower used in this study 11

9. IM7 cylinder with simulated propellant 12

10. Simulated propellant with square hollowed out 13

11. Modification of impactor to produce more puncture-type damage, and thus more fiber breakage 14

12. Damage caused by 78 ft•lb of impact energy with a 0.25-in-diameter impactor 14

13. Load-deflection plot of the impact event with 78 ft•lb of impact energy and a 0.25-in-diameter impactor 15

14. Damage caused by 50 ft•lb of impact energy with a 0.25-in-diameter impactor 16

15. Photomicrograph through surface crack on outer hoop ply showing fiber microbuckling 16

LIST OF FIGURES (Continued)

16. 50 ft•lb impact on IM7 cylinder with 0.25-in-diameter impactor 17

17. Method of excising and sectioning impact damage zones for subsequent microscopic examination of through-thickness damage 18

18. Damage caused by 50 ft•lb of impact energy with a 0.25-in-diameter impactor. IM7 fiber cylinder top row, T1100 fiber cylinder bottom row 19

19. Load-deflection plots of the impact events on both cylinders with 50 ft•lb of impact energy and the 0.25-in-diameter impactor 20

20. Cross-sectional photomicrographs of impact damage in IM7 fiber (left) and T1100 fiber (right) cylinders 21

21. Photograph of static indentation test methodology 23

22. Overlay of load-deflection plots of the static indentation tests with both types of fibers 24

23. Damage caused by static indentation testing. IM7 fiber specimens top row, T1100 fiber specimens bottom row 25

24. Thermography of damage caused by static indentation testing. IM7 fiber specimens top row, T1100 fiber specimens bottom row 26

25. Ultraviolet photographs of cross sections of static indentation specimens seen in figure 24 27

26. Cross sections of static indentation specimens seen in figures 24 and 25 28

27. Cross sections of select static indentation specimens 29

28. Load-deflection curves of two specimens with loading stopped after 'knee' in curve was noted 31

29. Thermography of damage caused by static indentation testing stopped after formation of 'knee' in load-deflection curve. IM7 fiber specimen left, T1100 fiber specimen right 32

LIST OF FIGURES (Continued)

30. Cross sections of static indentation specimens stopped after 'knee' in load-deflection curve. IM7 top, T1100 bottom. Closer views of delamination emanating from matrix crack at the hoop/helical interface highlighted 33

31. Cross section of static indentation specimen stopped before 'knee' in load-deflection curve 34

32. Setup of SBS test 35

33. Failed SBS test specimens 36

LIST OF TABLES

1. Some key properties of the two fibers used in this study (data from Hexcel and Toray) 1

2. Original winding sequence of cylinders to be used in this study 3

3. Resin mixture ratios used in this study 4

4. Cure cycle of cylinders used in this study 7

5. Results of SBS tests 36

LIST OF ACRONYMS

ASTM	American Society for Testing and Materials
BOLE	Booster Obsolescence and Lifetime Extension
DETA	diethylenetriamine
LAS	Launch Abort System
MSFC	Marshall Space Flight Center
SBS	short beam shear
UV	ultraviolet

TECHNICAL MEMORANDUM

A DAMAGE RESISTANCE COMPARISON OF WET-WOUND IM7 AND T1100 CARBON FIBER/EPOXY CYLINDERS

1. INTRODUCTION

As part of NASA's Booster Obsolescence and Lifetime Extension (BOLE) program, rocket motor cases made of Hexcel HexTow® IM7 carbon fiber are to be compared on a cost and performance basis to rocket motor cases made of Toray TORAYCA® T1100 carbon fiber. One aspect that needed addressing was the impact damage tolerance differences, if any, between rocket motor cases fabricated from each of these two types of carbon fiber. NASA Marshall Space Flight Center (MSFC) was given this task with a limited budget. Since residual case burst strength-after-impact testing was not feasible, this left damage resistance (i.e., the amount of damage formed due to an impact event) to be evaluated. The methodology for this task followed one done for the Launch Abort System (LAS) program,[1] in which hoop fiber breakage was the critical parameter after impact damage to be examined. Past studies by Nettles have shown that the critical parameter that will determine the residual burst strength of a pressure vessel is hoop fiber breakage, with delaminations and matrix damage having no effects.[2] Thus, this study is concerned with a comparison of the amount of fiber breakage in two identical wet-wound cylinders, one made with IM7 fiber and the other made with T1100 fiber.

The rationale behind this testing program was that if the T1100 fiber was as damage tolerant (or more so) as the IM7 fiber when used in a wet-wound structure, then the results of a previously conducted damage tolerance study[3] on rocket motor cases that used IM7 fiber could be used.

Table 1 shows some properties of the two fibers used in this study, as given by each vendor. The IM7 fiber has long been one of the composite industry's standards and is well characterized; while the T1100 fiber is a newer generation carbon fiber with higher tensile strength and modulus, but not as much characterization.

Table 1. Some key properties of the two fibers used in this study (data from Hexcel and Toray).

Fiber Property	Hexcel IM7	Toray T1100
Tensile Strength	825 ksi	1,017 ksi
Tensile Modulus	40.0 Msi	47.0 Msi
Strain to Failure	1.8%	2.0%
Density	1.78 g/cm^3	1.79 g/cm^3
Filament Diameter	5.2 microns	5.0 microns

The IM7 fiber has a "Hexcel type G" sizing agent (i.e., fiber surface treatment) applied and the T1100 fiber had a "Toray type 5" sizing agent applied. As a result, different surface treatments were used on the two types of fiber. These sizing agents were chosen by each manufacturer to give the best fiber/matrix bond with epoxy resin.

This paper presents the results of impact damage testing on two cylinders: one made from each type of fiber. Results are presented in a chronological order of sorts, since changes had to be made to the original lay-up of the cylinders due to a problem in the manufacturing process; changes in impact methodology were then needed in order to produce fiber damage that could be more easily compared between the two cylinders.

It must be emphasized that the results of this study are only to compare the two fiber types and that the impact damage data produced here will not scale to a much thicker cylinder such as the BOLE rocket motor case. Damage tolerance data on full-scale rocket motor cases made of IM7 fiber are available[3] and it is assumed that if the T1100 fiber is as damage resistant (or more so) than the IM7 fiber when in a wet-wound configuration, then the IM7 full-scale damage tolerance data can confidently be used for comparison to a full-scale rocket motor case made of T1100 fiber.

2. MANUFACTURE OF TEST ARTICLES

2.1 Overview

The Northrop Grumman-made CLRF–100 epoxy resin was used in the manufacturing of both IM7 fiber and T1100 fiber cylinders. The cylinders were made with a diameter of 36 in and a cylindrical width of 18 in. Originally the planned lay-up consisted of 22 plies, as shown in Table 2. To conserve time, each band width of 0.4 in was a double layer of tows (8 tows versus 4 tows). This proposed lay-up was to give an approximate cylinder thickness of 0.39 in.

Table 2. Original winding sequence of cylinders to be used in this study.

Sequence	Material	Orientation	Winding Parameters				
			Band Width (in)	Tow Tension (lb) (4.5-5)	Resin Content (29.5–33.5 % wt)	Angle (deg)	Wind Angle Tolerance
1	IM7/T1100	Helical	0.4	4.75	32.9	±33	+/- 2
2	IM7/T1100	Hoop +	0.4	4.75	32.9	-88	+/- 2
3	IM7/T1100	Hoop -	0.4	4.75	32.9	+88	+/- 2
4	IM7/T1100	Helical	0.4	4.75	32.9	±33	+/- 2
5	IM7/T1100	Helical	0.4	4.75	32.9	±33	+/- 2
6	IM7/T1100	Hoop+	0.4	4.75	32.9	-88	+/- 2
7	IM7/T1100	Helical	0.4	4.75	32.9	±33	+/- 2
8	IM7/T1100	Helical	0.4	4.75	32.9	±33	+/- 2
9	IM7/T1100	Hoop +	0.4	4.75	32.9	+88	+/- 2
10	IM7/T1100	Helical	0.4	4.75	32.9	±33	+/- 2
11	IM7/T1100	Helical	0.4	4.75	32.9	±33	+/- 2
12	IM7/T1100	Hoop +	0.4	4.75	32.9	-88	+/- 2
13	IM7/T1100	Helical	0.4	4.75	32.9	±33	+/- 2
14	IM7/T1100	Helical	0.4	4.75	32.9	±33	+/- 2
15	IM7/T1100	Hoop +	0.4	4.75	32.9	+88	+/- 2
16	IM7/T1100	Hoop -	0.4	4.75	32.9	-88	+/- 2
17	IM7/T1100	Helical	0.4	4.75	32.9	±33	+/- 2
18	IM7/T1100	Helical	0.4	4.75	32.9	±33	+/- 2
19	IM7/T1100	Hoop +	0.4	4.75	32.9	+88	+/- 2
20	IM7/T1100	Hoop -	0.4	4.75	32.9	-88	+/- 2
21	IM7/T1100	Helical	0.4	4.75	32.9	±33	+/- 2
22	IM7/T1100	Helical	0.4	4.75	32.9	±33	+/- 2

As the first IM7 fiber cylinder was being wound, a problem with the mandrel necessitated that the winding be stopped after the 9th ply had been wound. It was determined that this cylinder should be cured as-is in order to conserve the part. The T1100 fiber cylinder was then wound the same way, stopping at the 9th ply rather than manufacturing to the full thickness, as a direct comparison of cylinders was desired with the only difference being the type of fiber used. Since a comparison of fiber breakage was the response variable of interest, and since even the originally planned 22-ply full-thickness cylinder would not come close to truly representing the very thick BOLE case, this was deemed acceptable for the purposes of this study.

As a result of this change in parameters, the final two test cylinders were manufactured following the lay-up shown in Figure 1. The nominal thickness of the two cylinders were 0.2 in. (For comparison, the nominal thickness of the LAS cylinder was 0.4 in and the nominal thickness of the final BOLE case is to be about 1.4 in.)

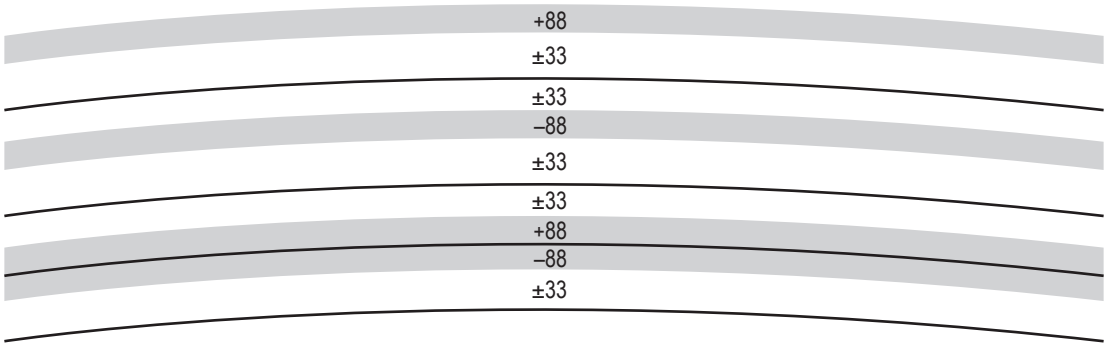

Figure 1. Schematic of cylinder lay-ups used for impact testing in this study.

2.2 Materials

2.2.1 Resin

The resin mix criteria set by Northrop Grumman is shown in Table 3. Each batch of resin made for the manufacturing of these cylinders followed these parts-by-weight mixture ratios.

Table 3. Resin mixture ratios used in this study.

Parts by Weight	Description
76.78–77.18	CLRF–100 Modified Epoxy Resin
20.66–21.06	Diethylenetriamine (DETA) Curing Agent
2.11–2.21	Curing Agent Catalyst

A resin bath was used to apply the CLRF–100 resin mix to the fiber rovings. By using a scale and adjusting the doctor blade on the resin bath, the resin content was set to 32.9 wt%.

2.2.2 Fiber

IM7 and T1100 fibers were used to compare the impact damage resistance. IM7 is a carbon fiber that is currently widely used in industry. T1100 is a newer generation carbon fiber with improved fiber properties. Some key properties of these fibers were given in Table 1. Each cylinder was wound from a single fiber lot from each vendor.

2.2.3 Mandrel

The mandrel was made of sand and a binder material from Advanced Ceramics Manufacturing. This mixture creates a hard solid that is machinable. The case dimensions were applied to the mixture and bonded to a 2.5-in-diameter steel shaft. The sand/binder mix is water soluble, so after the part is made and cured, the mandrel can be removed with water to leave the part behind. A picture of the sand mandrel is shown in figure 2.

Figure 2. One of the two sand mandrels used to manufacture the cylinders used in this study.

2.3 Dry Wind

A dry wind (i.e., winding without resin), which is usually done to confirm the pattern of the fiber on the mandrel before resin is added, was performed for this project. Pictures of the helical-ply dry wind and the hoop-ply dry wind are shown in figure 3. Once the dry wind was completed and the winding pattern verified, the dry fiber was stripped from the mandrel before the wet-winding process began.

Figure 3. Dry winding to test filament winder settings before the actual wet winding is performed. Helical pattern is shown on left and hoop pattern is shown on right.

The helical patterns followed a ±33° angle with a +/- 2° tolerance while the hoops followed a ±88° angle with a +/- 2° tolerance.

2.4 Cure Cycle

The cylinders were rotisserie cured in an oven using the cure cycle in Table 4. Each cure ran smoothly with no interruptions. This cure followed Northup Grumman-developed steps for a 36-in rocket motor case.

Table 4. Cure cycle of cylinders used in this study.

Cure Cycle					
Step	Temperature Set Point [°F]	Temperature Tolerance	Temperature Ramp Rate [°F/min]	RPM	Dwell Time [hrs]
1	Ambient	–	–	5	72
2	110	105 – 120	5	5	16
3	185	175 – 195	2.5	5	6
4	300	290 – 310	2.5	5	2
5	285	275 – 295	0.5	5	23
6	150	–	10	5	–
7	End	–	–	–	–

2.5 IM7 Fiber Cylinder Manufacture

The first 8 layers were wound using the parameters detailed in Table 2. However, the mandrel was discovered to be broken after layer 8. A relatively quick fix was done to get one more layer onto the mandrel. To not lose the part completely, the cure cycle was started after layer 9, a hoop layer, was wound. Figure 4 shows the IM7 case after layer 9 and before the peel ply was added.

Figure 4. Wet-wound IM7 fiber cylinder after addition of ninth layer.

Figure 5 shows the wet-wound cylinder being placed into the large oven. Note the yellow peel ply placed on the outside of the cylindrical portion (i.e., non-domed area) of the case. The shaft was inserted into the back of the oven, where a motor provided continuous rotation during cure.

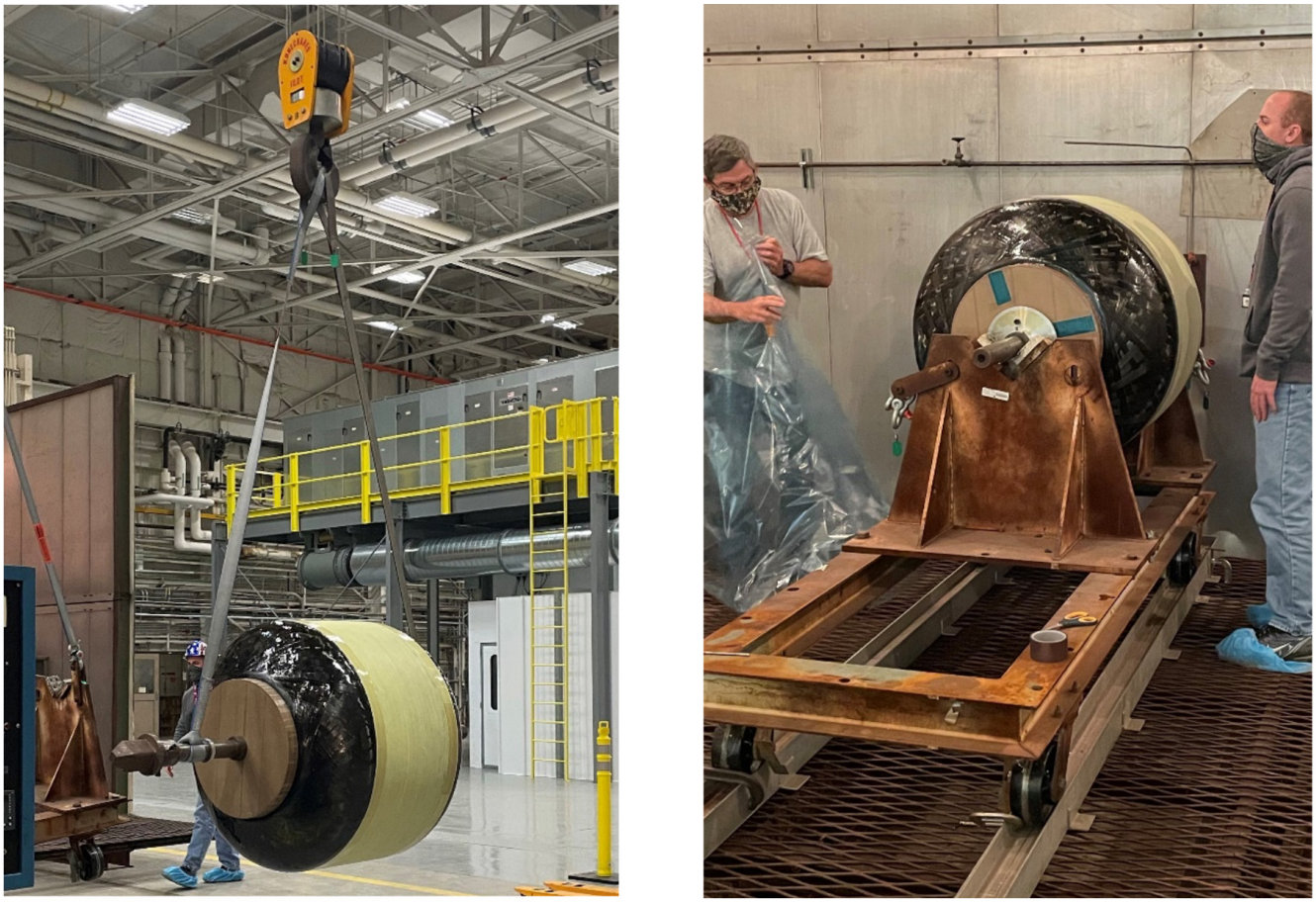

Figure 5. Wet-wound IM7 fiber cylinder being carried to (left) and placed into (right) the oven for curing.

2.6 T1100 Fiber Cylinder Manufacture

To compare the two cylinders as evenly as possible, the T1100 cylinder was wound using the same manufacturing steps as the IM7 fiber case (i.e., stopping at the ninth ply). Cross-sections of each of the two cylinders in the hoop direction and in the helical direction are shown in figures 6 and 7. These cross sections were excised from various areas in the cylinders throughout this program but are presented here at the beginning of this paper to give the reader an idea of the microstructural morphology of the two undamaged cylinders. The hoop fibers—one at the top, one near the center, and two near the bottom—are labeled in the first photographs of figure 6.

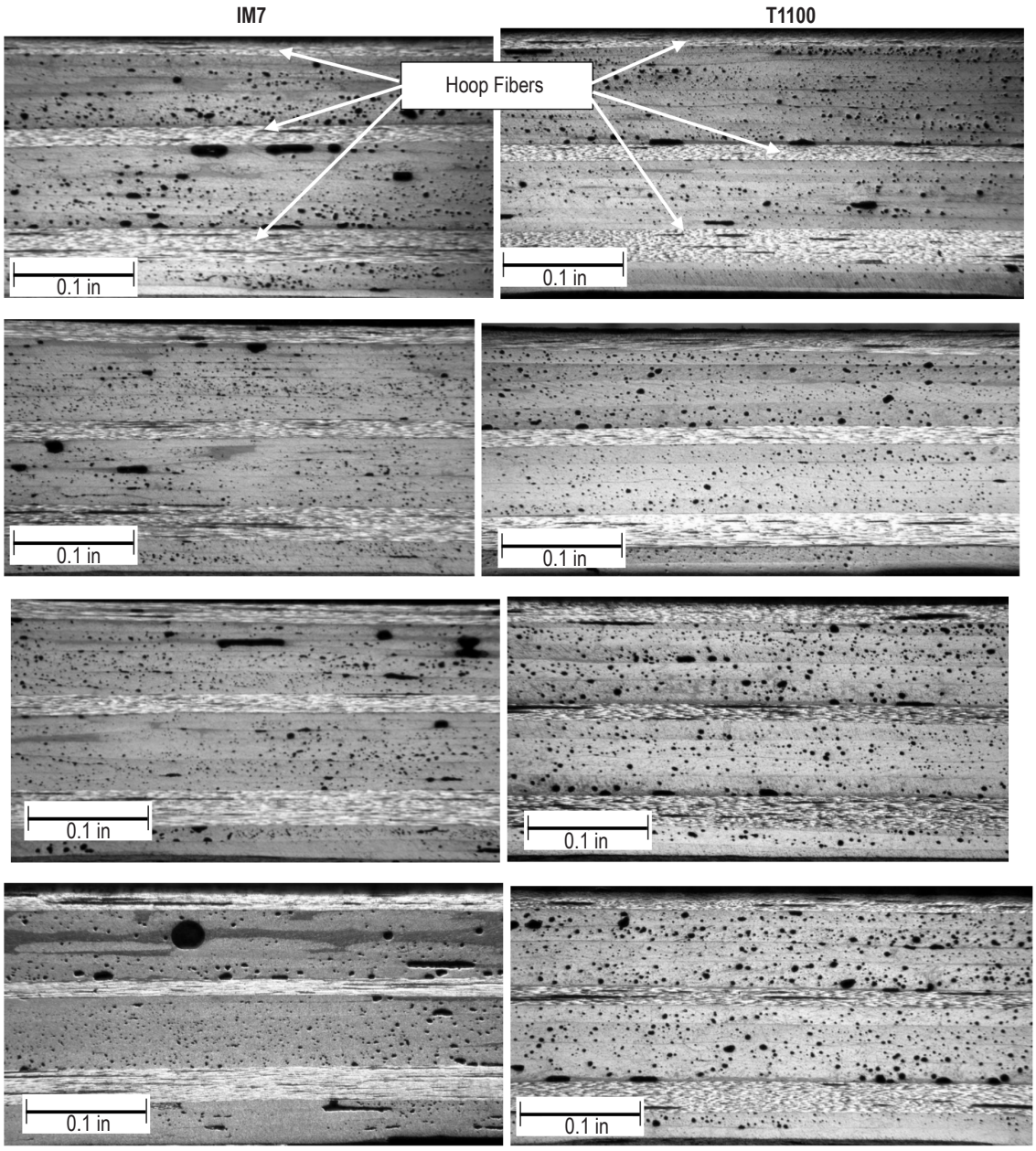

Figure 6. Undamaged cross sections in the hoop direction.

Layers parallel to the cross-sectional cut can be seen in photomicrographs as bright layers. Thus, in figure 6, the hoop fibers can clearly be seen; and in figure 7, the +33° helical fibers can clearly be seen. Note how the helical-direction cross sections are less similar looking to one another than the hoop-direction cross sections. This is due to the helical stacking sequence varying from point to point across the cylinder due to the over/under winding pattern, as can be seen by the diamond pattern in figure 3. Unless these diamonds lie perfectly over each other for all layers, then some areas will have +33° (or -33°) fibers laying atop one another rather than alternating ±33° layers.

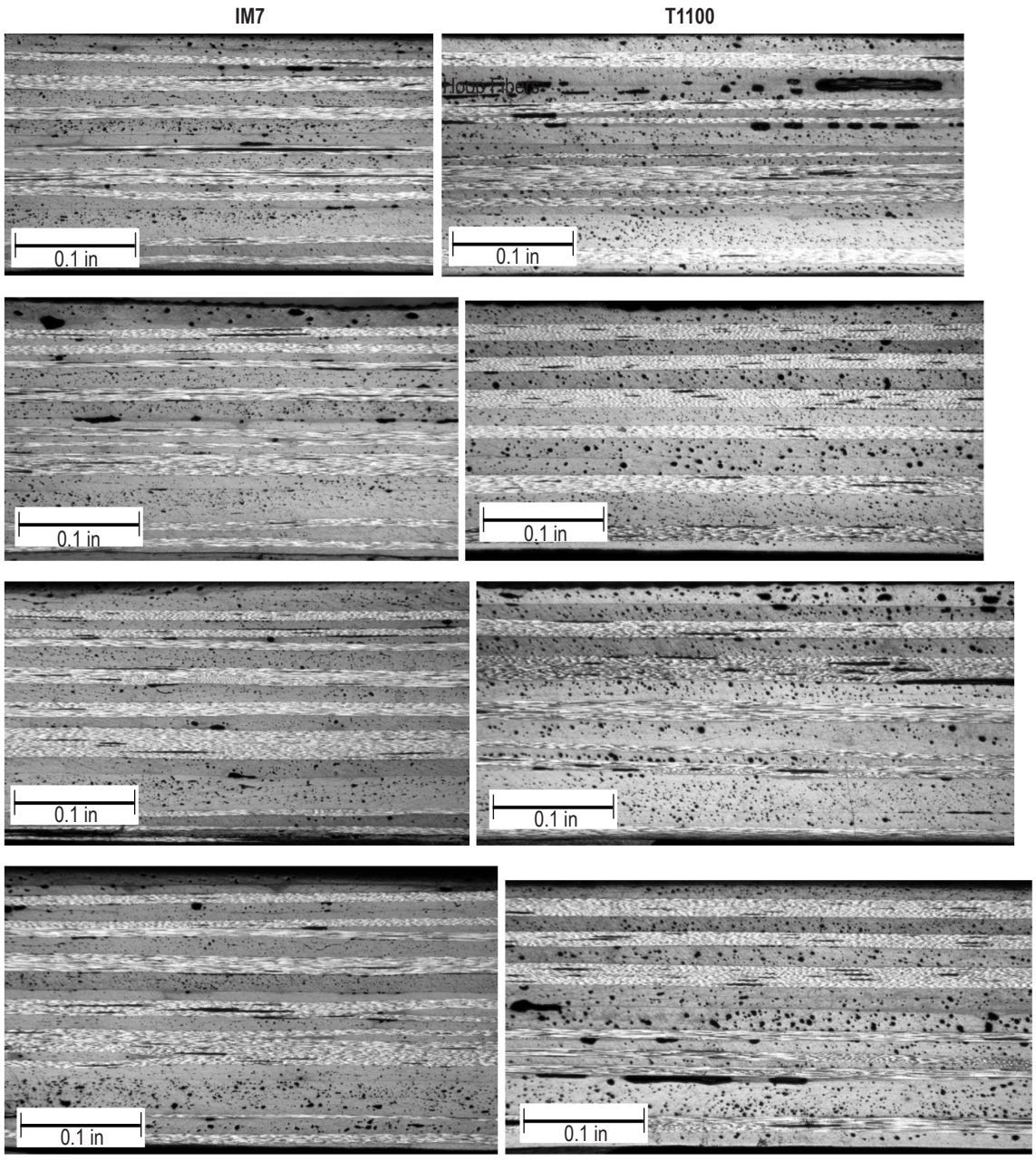

Figure 7. Undamaged cross sections in the helical direction.

The typical high level of porosity that is seen in wet-wound structures is evident, and the two cylinders appear to be of similar quality.

3. IMPACT TESTING

The cylinders were impacted using an instrumented drop-weight tower that was positioned over the cylinders. A photograph of the drop tower is shown in figure 8. Initially an impactor of 0.5-in diameter was used since that size is most common and what was mostly used in the LAS study.[1]

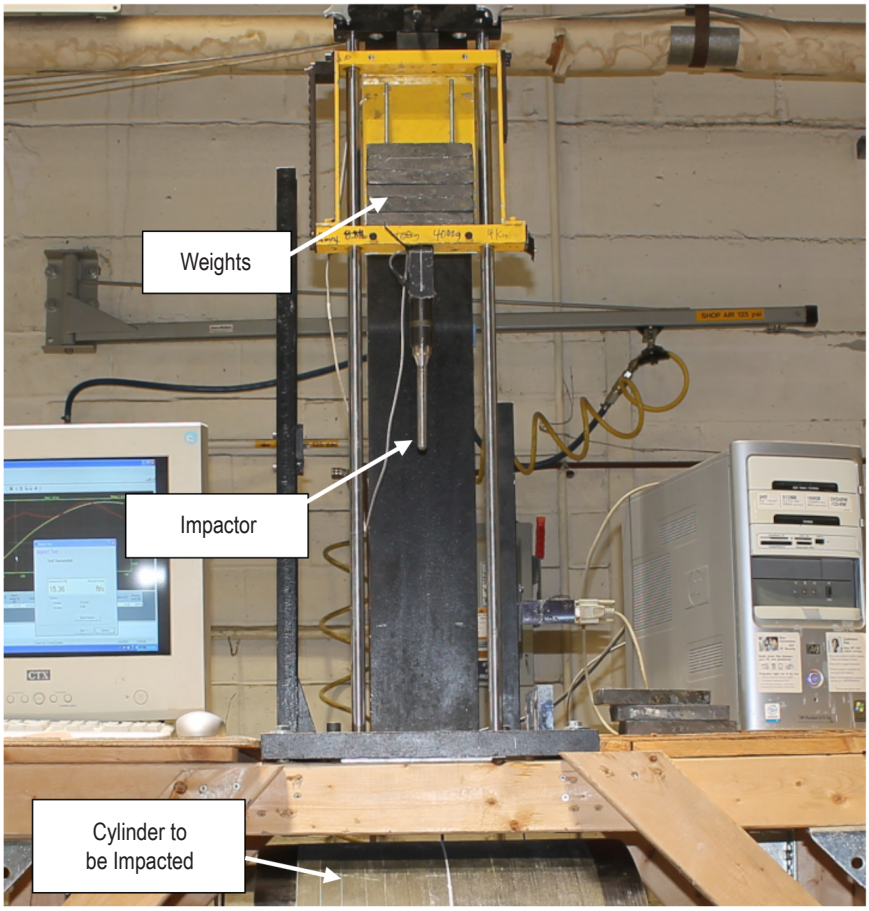

Figure 8. Drop tower used in this study.

In order to prevent large deflections and thus have only localized fiber damage, which is easier to ascertain and uses less area of the cylinder, simulated propellant was used on the inside of the cylinder as it was in the LAS study.[1] A photograph of the IM7 cylinder with the simulated propellant pressing against the inner surface of the cylinder is shown in figure 9. Note the sand-bags that were placed in the cylinder prior to impact, in order to add more stabilization to the cylinder as it sits in the wooden cradle structure.

The simulated propellant was placed against the unimpacted surface (i.e., inside) of the case so that approximately 4 × 4 in under the impact site is supported in a so-called 'plate on an elastic foundation' configuration. This was accomplished by pressing the inert propellant against the inside surface of the case and having the inert propellant rigidly supported with respect to this surface. The device used to do this consisted of the following three parts: (1) the inert propellant, (2) a spanner beam, and (3) a tightening block, as pictured in figure 9. The inert propellant was excess taken from the inside of a 5.75-in pressure vessel that was slated to be tested for a damage tolerance program at NASA MSFC in the early 1990s. In order to press the inert propellant to the surface of the case, a 2-by-4 wooden beam was used as a spanner beam across the diameter of the case. The spanner was fastened to the tightening block, such that two nuts could be turned to raise the 2-by-4 spanner and thus apply pressure to the inert propellant.

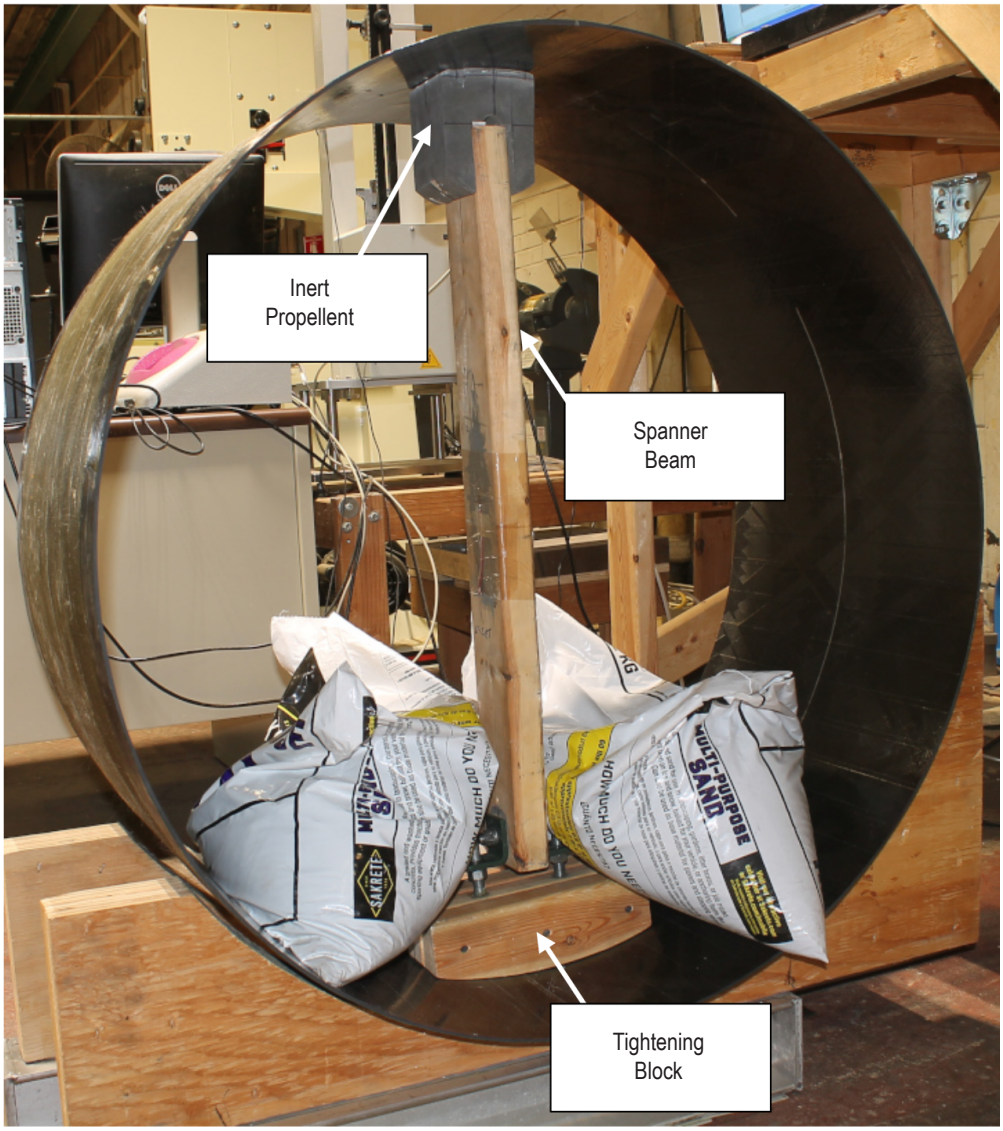

Figure 9. IM7 cylinder with simulated propellant.

The first impact was attempted with 118 ft•lb of impact energy with the 0.5-in-diameter impactor and caused a maximum point load of 3,298 lb. Despite this severe level of impact, there was little damage to the cylinder and certainly no fiber breakage. In an attempt to cause more local flexure, and thus hopefully fiber breakage, the simulated propellant was hollowed out in a 2.75-in square to allow more flexure in the wall of the rocket motor case directly below the impactor. A picture of the hollowed-out inert propellant is shown in figure 10. This did not enhance fiber breakage and no fiber breakage was seen at 123 ft•lb of impact energy.

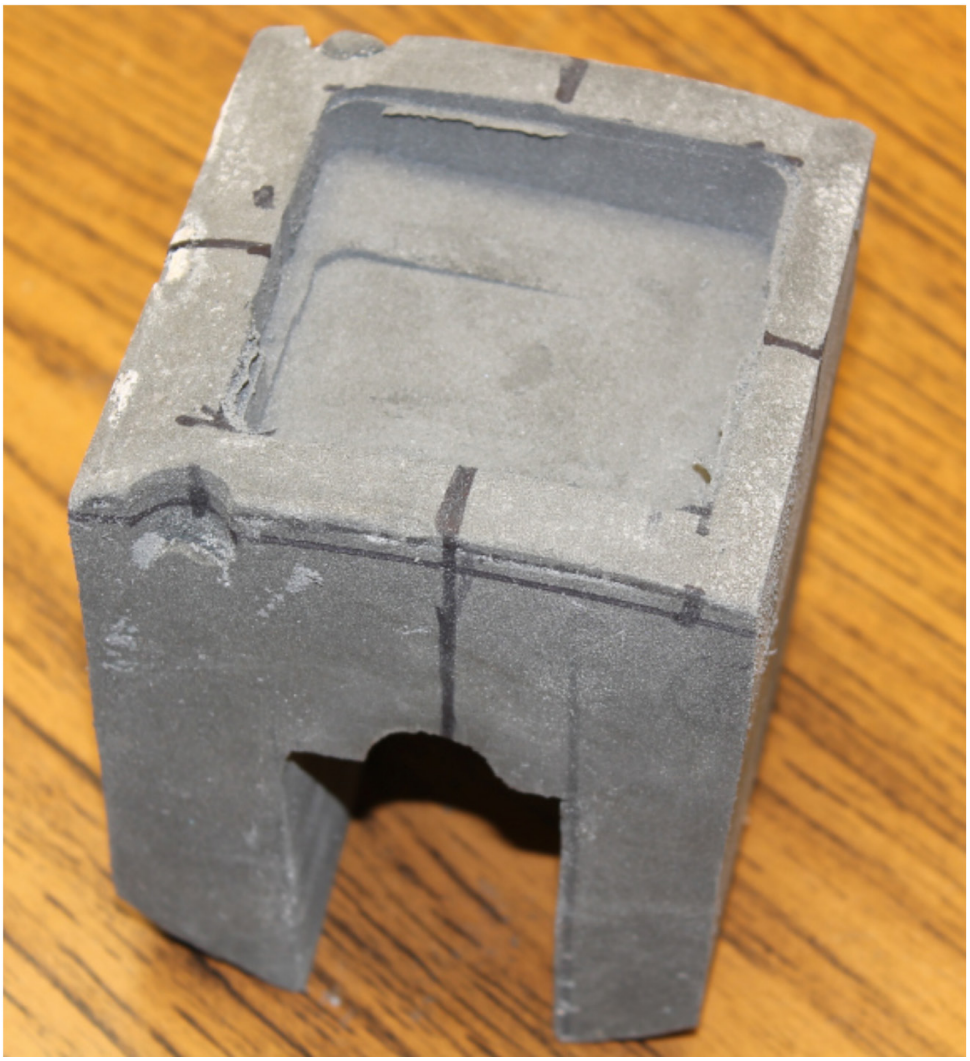

Figure 10. Simulated propellant with square hollowed out.

At this point it became clear that more of a puncture-type impact may be needed, since in the LAS study a 'protruding bolt' produced the most fiber breakage.[1] The 'protruding bolt' adapter used in the LAS study was used again in this study. A 1/4-in bolt was inserted into the adapter and had its end rounded, as shown in figure 11. This essentially gave a 0.25-in-diameter impactor rather than a 0.5 in impactor.

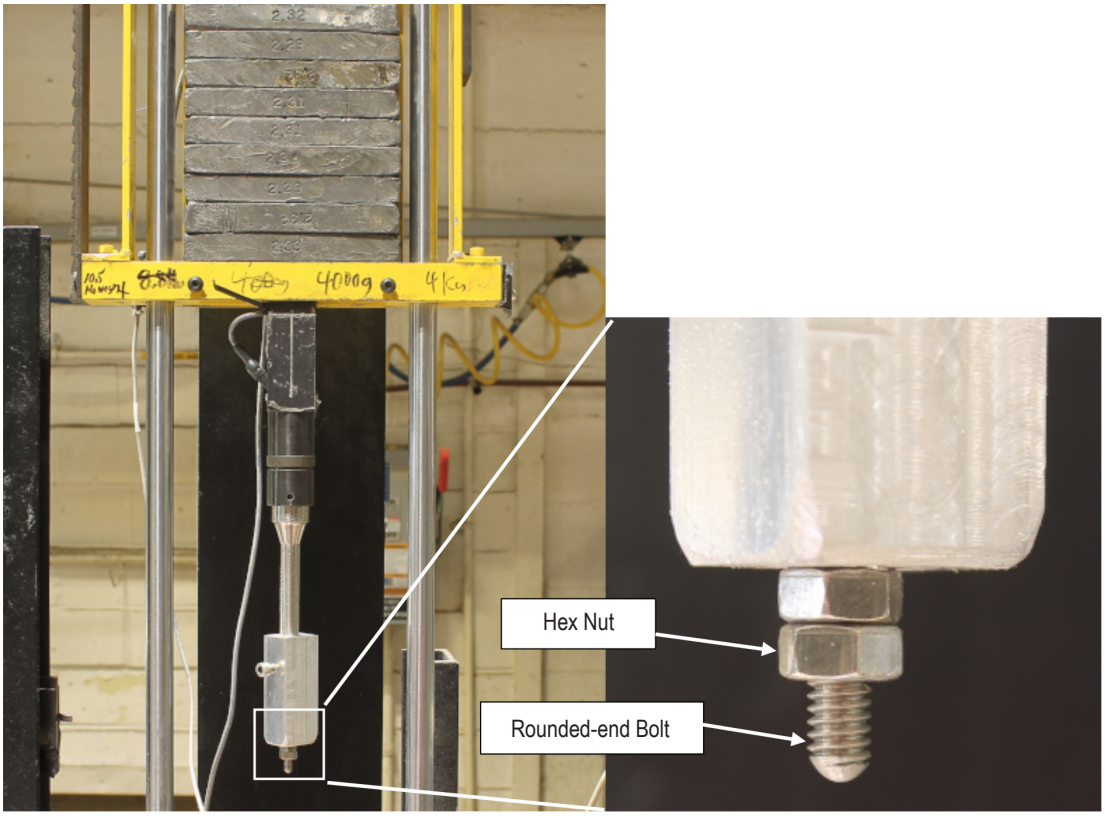

Figure 11. Modification of impactor to produce more puncture-type damage, and thus more fiber breakage.

The first impact attempted with the bolt was made at 78 ft•lb of impact energy and most definitely caused fiber breakage. The impactor penetrated the cylinder enough that there was no rebound of the impactor and it essentially stuck into the cylinder. A photograph of the damage from this impact is shown in figure 12.

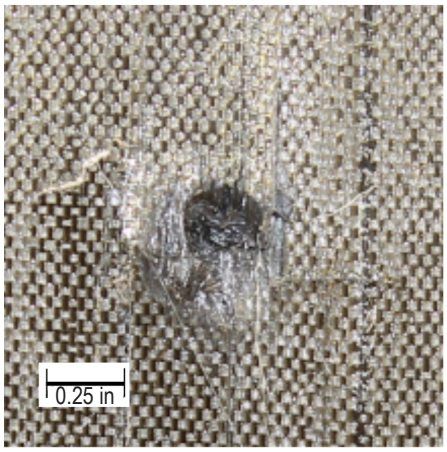

Figure 12. Damage caused by 78 ft•lb of impact energy with a 0.25-in-diameter impactor.

The load-deflection plot of the 78 ft•lb impact event with the 0.25-in-diameter impactor is shown in figure 13. It can be seen that the bolt penetrated the cylinder with the first hump and then there was a secondary impact as the nut on the bolt came into contact with the cylinder.

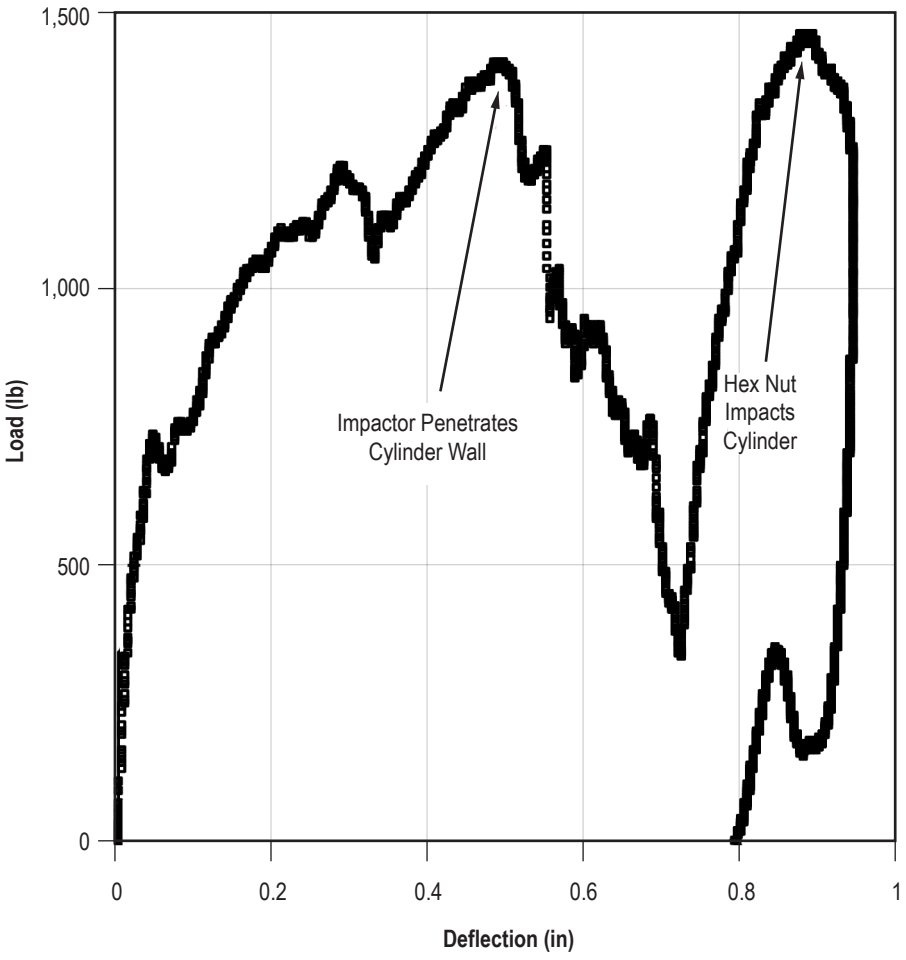

Figure 13. Load-deflection plot of the impact event with 78 ft•lb and the 0.25-in-diameter impactor.

The impact energy was reduced to 50 ft•lb and, using this lower impact energy level, the impacting crosshead did rebound and there was visible damage as shown in figure 14. Note that there is a crack on the surface running perpendicular to the hoop plies. This was apparent on many of the impacts on the IM7 fiber cylinder. An impact damage zone was excised from the IM7 cylinder and sectioned trough the surface crack as noted in the figure. The method used to excise the impact damage zone will be presented later in the paper.

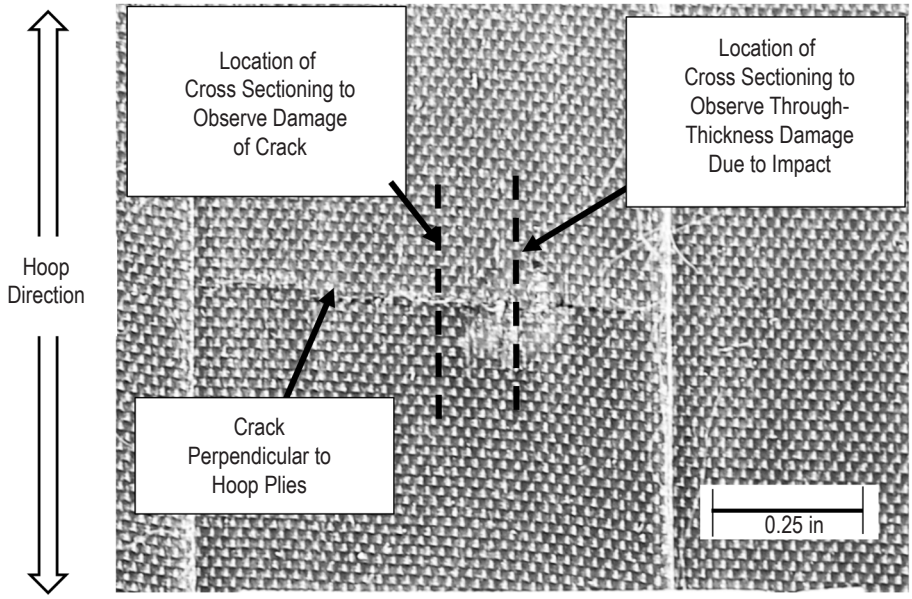

Figure 14. Damage caused by 50 ft•lb of impact energy with a 0.25-in-diameter impactor.

The resulting photomicrograph showing the fiber microbuckling damage in the outer hoop ply is shown in figure 15. This fiber microbuckling is an indication of compressive failure and has been seen by the author when impacting flat plates. The microbuckling occurs because the top surface (i.e., the impacted side) briefly experiences a compressive load, which is apparently large enough to cause compressive fiber failure, at the beginning of impact. This compressive load continues until large deformation and membrane stretching begins to occur, at which point the entire area (i.e., the top and bottom of the cylinder wall) is under a tensile load.

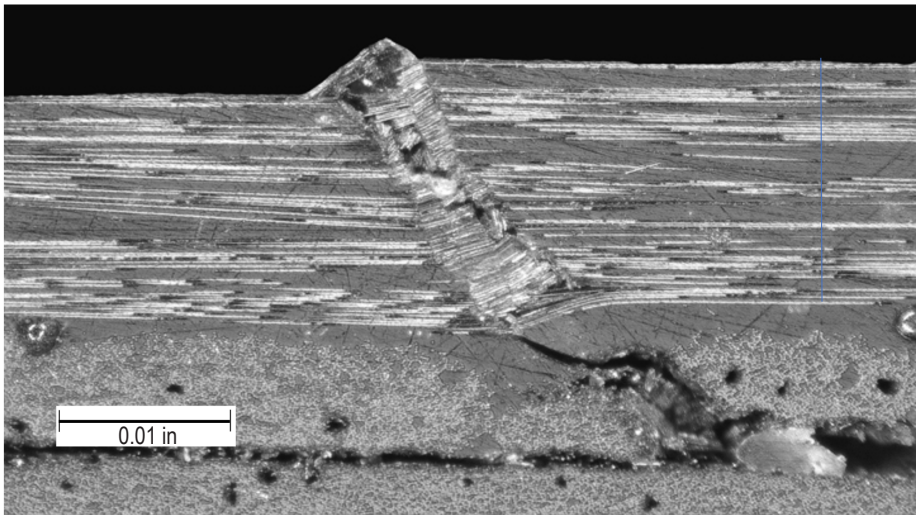

Figure 15. Photomicrograph through surface crack on outer hoop ply showing fiber microbuckling.

Another of these 50 ft•lb impacts was excised from the cylinder and sectioned through the center of the damage zone in the hoop direction, as noted in figure 14. The resulting photomicrograph is shown in figure 16. At this area of the damage zone, the outermost hoop ply is punctured and severe damage is seen up to the centermost hoop ply, which appears to be broken.

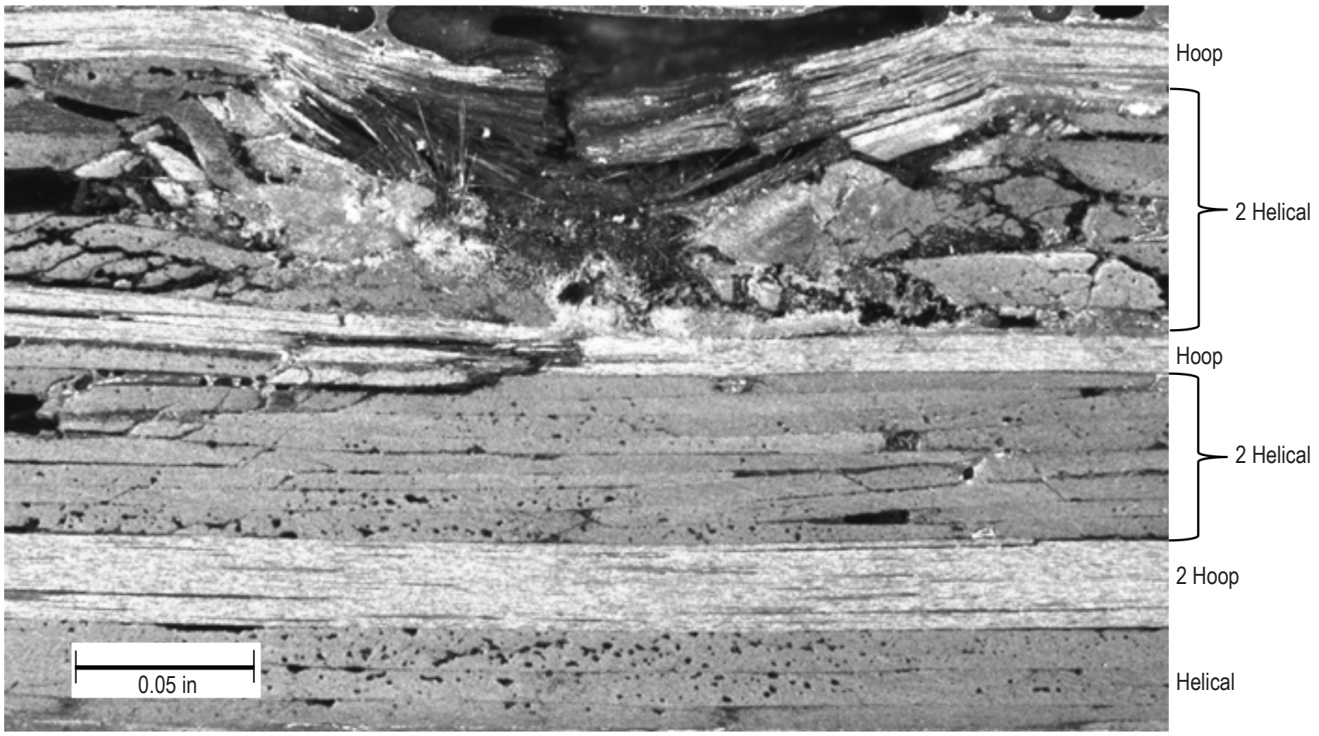

Figure 16. 50 ft•lb impact on IM7 cylinder with 0.25-in-diameter impactor.

To excise and section the impact damage zones, a square around the impact site was marked off and two holes drilled diagonally across from one another. A jig saw was inserted into these holes and cuts made along the marked off square to excise the impact zone. Since the impact event was highly localized, the cut-outs did not affect other impacts performed on the cylinders. The excised square was then sectioned through the damage zone with a wafering blade. The cut edges with the impact damage were then polished up to a grit of 1200 for viewing under a microscope. Some photographs of this excising methodology are shown in figure 17.

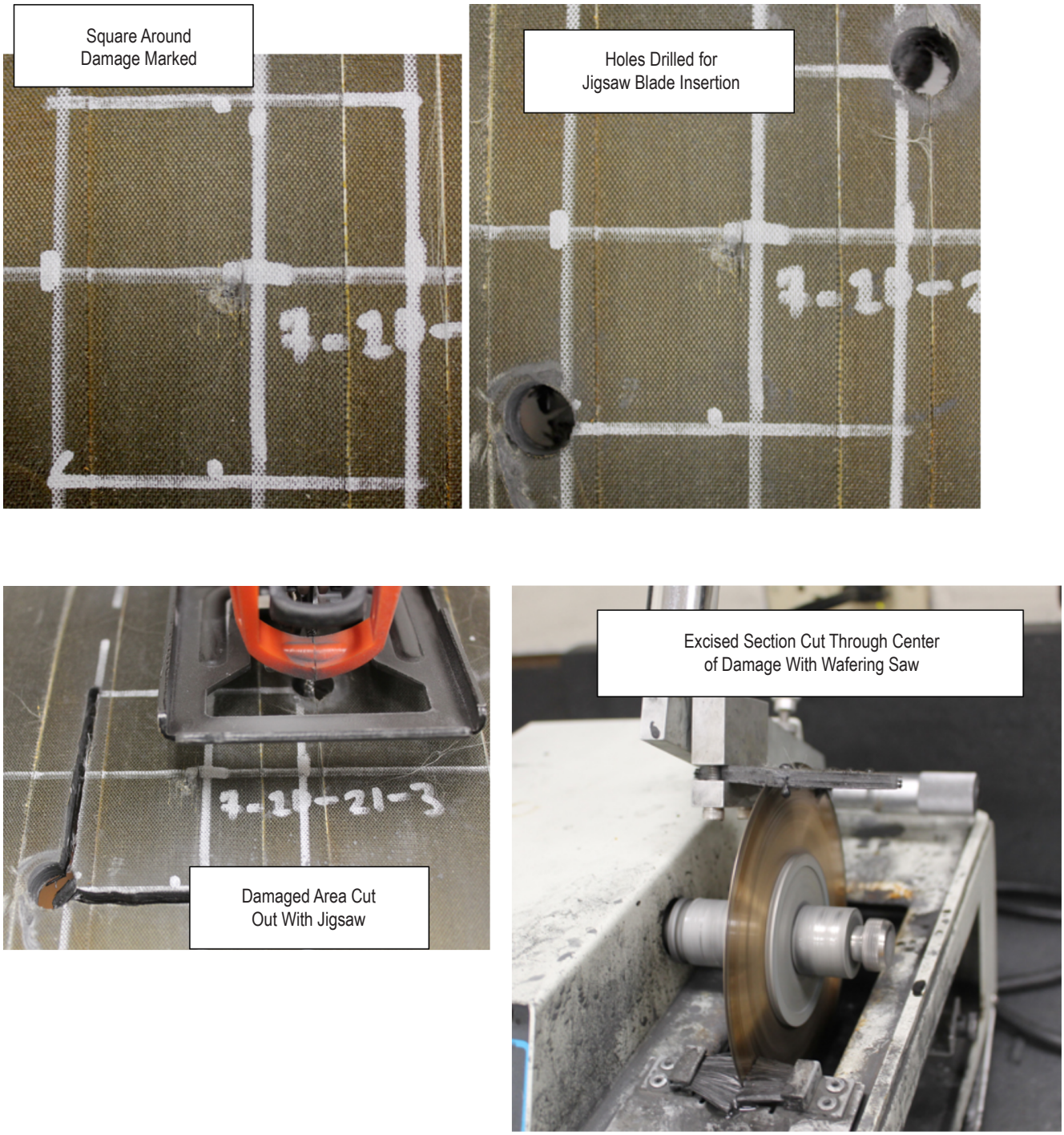

Figure 17. Method of excising and sectioning impact damage zones for subsequent microscopic examination of through-thickness damage.

4. RESULTS OF IMPACT TESTING

Having settled on this impact energy level (≈50 ft•lb), four impacts were conducted on each of the two cylinders and the impact damage zones sectioned on each of the cylinders. Since fiber breakage was the variable of interest, the researchers decided to section the impact zones in the direction of the helical plies. The research team hoped that the depth of fiber damage would be more easily visible since there are more helical plies closer to the surface, as fiber damage can only be seen when cut parallel to the fibers.

Typical visual damage for two each of the IM7 and T1100 cylinder impacts are shown in figure 18. In general, the T1100 fiber cylinder shows less visible impact damage than the IM7 fiber cylinder.

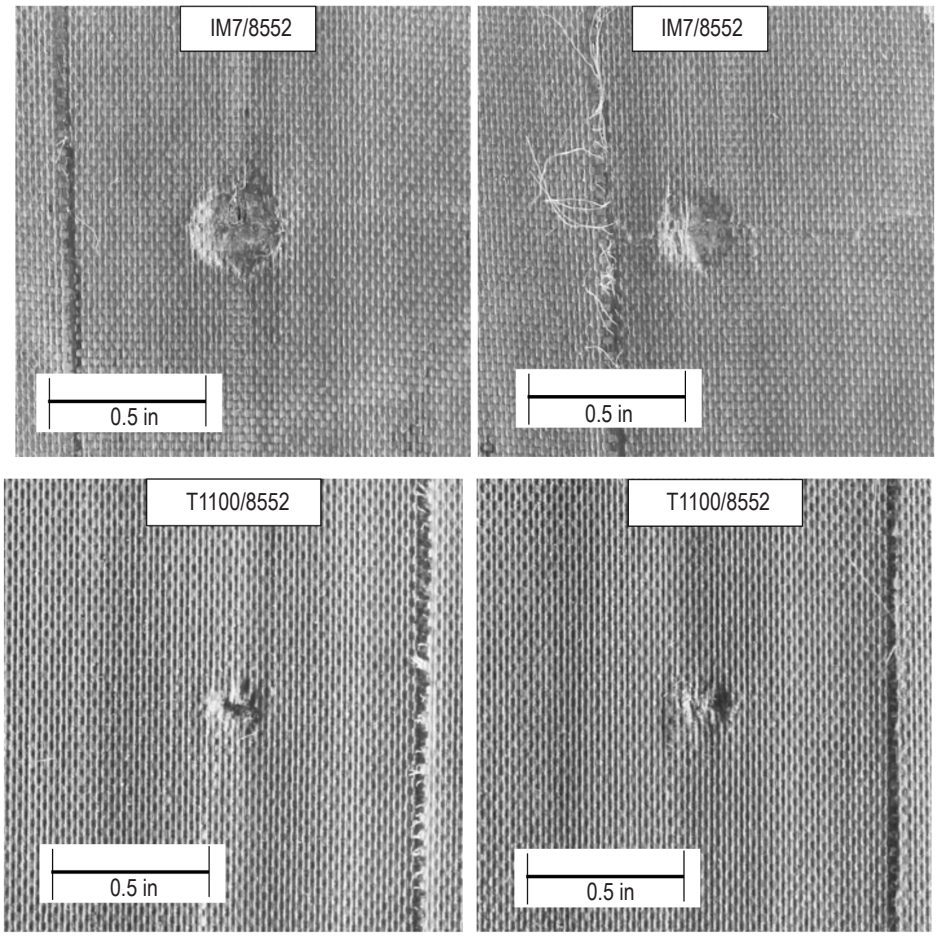

Figure 18. Damage caused by 50 ft•lb of impact energy with a 0.25-in-diameter impactor. IM7 fiber cylinder top row, T1100 fiber cylinder bottom row.

The load-deflection curves of some of the impact events are all superimposed upon one another in figure 19. The IM7 data are in black and the T1100 data are in gray. The data are quite repeatable and the only noticeable difference between the two fibers is that the T1100 fiber could sustain a slightly higher maximum load of impact. This finding, coupled with the visual damage results seen in figure 18, indicates that the T1100 cylinder is slightly more damage resistant.

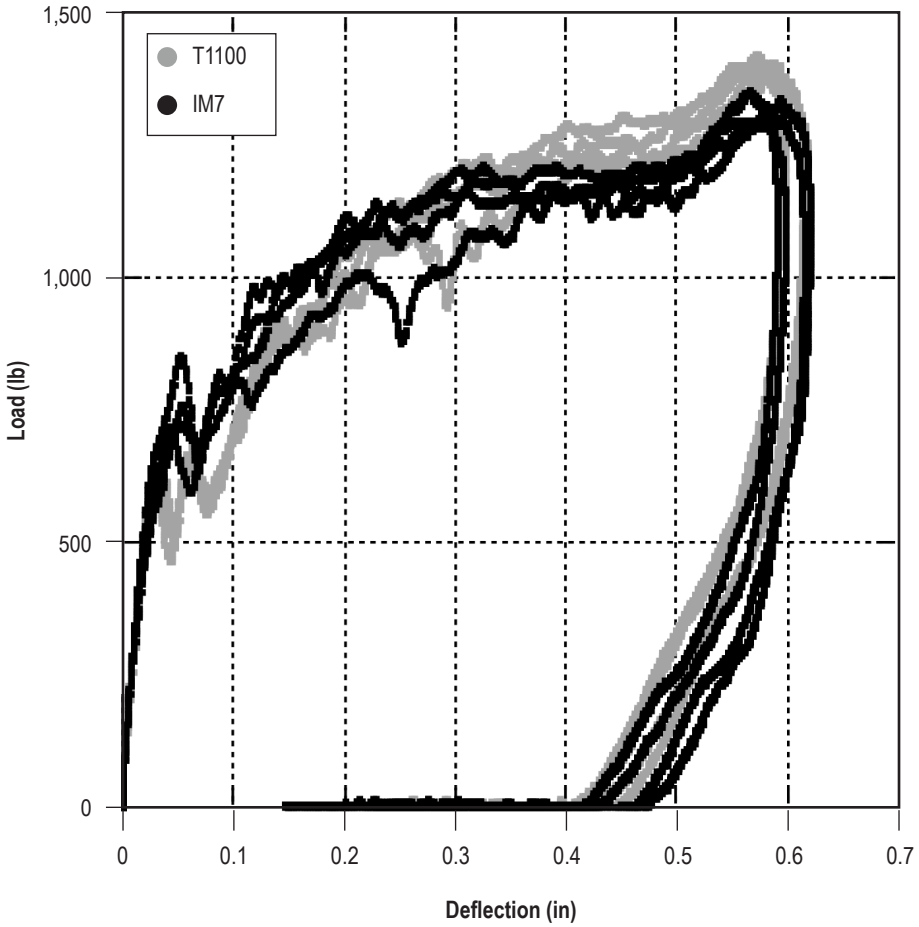

Figure 19. Load-deflection plots of the impact events on both cylinders with 50 ft•lb of impact energy and the 0.25-in-diameter impactor.

Photomicrographs of the damage using cross-sectional microscopy are shown in figure 20. The IM7 fiber specimens are shown in the left column and the T1100 fiber specimens are shown in the right column. These cross sections are in the helical fiber direction.

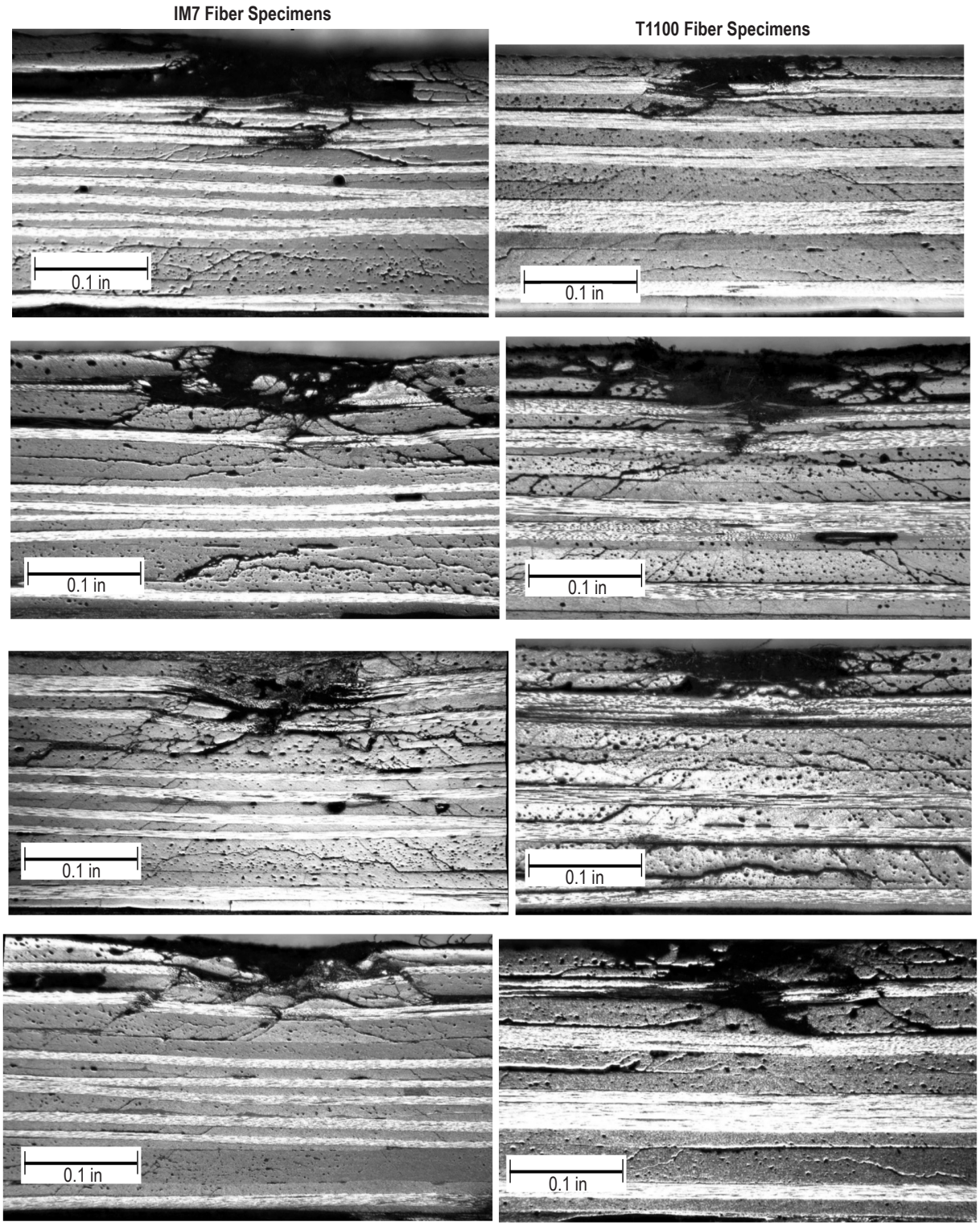

Figure 20. Cross-sectional photomicrographs of impact damage in IM7 fiber (left) and T1100 fiber (right) cylinders.

From the photomicrographs in figure 20 alone, it was difficult to ascertain if the T1100 fiber had more damage resistance compared to the IM7 fiber. The research team hoped that the top two helical plies that were parallel to the plane of the photograph (the brighter plies that show fiber damage) would show more difference in fiber breakage; but either more specimens or a different impact energy level was needed. About all that the researchers could deduce from the results shown in figure 20 was that there was no obvious difference in damage resistance between the two types of fibers.

At this point in the testing program, two things became evident:

(1) Since the impacts were only at the center of the cylinder and spaced at least 8 in apart, a limited number of impacts could be performed on each cylinder.

(2) Trying to compare the damage by cutting in the helical direction was difficult, since the stacking sequence varied from point to point in the cylinder. This was because the helical plies were essentially like a large woven ply, in which patches of the layers would be in an over-and-under configuration. This configuration formed the diamond shapes easily seen on the inner surface of the cylinder in figure 3. Note the difference seen in figures 6 and 7, in which the hoop-direction cross sections were more consistent in appearance than the helical-direction cross sections.

A solution was chosen in which damage resistance specimens could be cut from the cylinder before inflicting damage on them. This gave a much larger area of cylinder from which to get specimens, since the restrictions of the impact zones having to be at the center of the cylinder and 8 in away from each other were no longer applicable. The boundary conditions would obviously be different from the impact tests conducted with the drop-weight tower, but since a direct comparison of damage to fibers was the variable of interest and the boundary conditions of a full-scale rocket motor case could not be achieved anyway, using a static indentation technique was deemed acceptable.

A static indentation test consists of transversely loading the specimen with an indenter similar to the ones used for drop-weight impact testing. It is essentially a slow-motion impact event and has been found by Nettles and Douglas to give similar results to drop-weight impact tests.[4] The methodology used to perform these tests is presented in the following section.

5. STATIC INDENTATION TESTING

Since the only goal of this study was to ascertain any damage resistance difference in the type of fiber used, it was decided that using static indentation tests to represent impact damage would be more beneficial since many more specimens could be excised from the cylinders. In addition, the cuts to examine damage were made in the hoop fiber direction since these cross sections were much easier to compare due to the consistency of the appearance of the cross sections. By using static indentation, the transverse load could be more easily adjusted such that the hoop ply nearest to the center of each specimen could be damaged.

A photograph of the static indentation test setup is shown in figure 21. The static indentation tests were conducted using an Instron® 10,000-lb capacity load frame. 4 × 4 in specimens were excised from the cylinders and used for testing. A support platform made of wood and aluminum was used to support the specimens with all edges simply supported. The transverse loading rate was set at 0.5 in per minute. The test was manually stopped after a predetermined load had been reached. Through trial and error, a maximum transverse load of about 2,200 lb was chosen for all of the specimens. The cross-head displacement and load were recorded for each test.

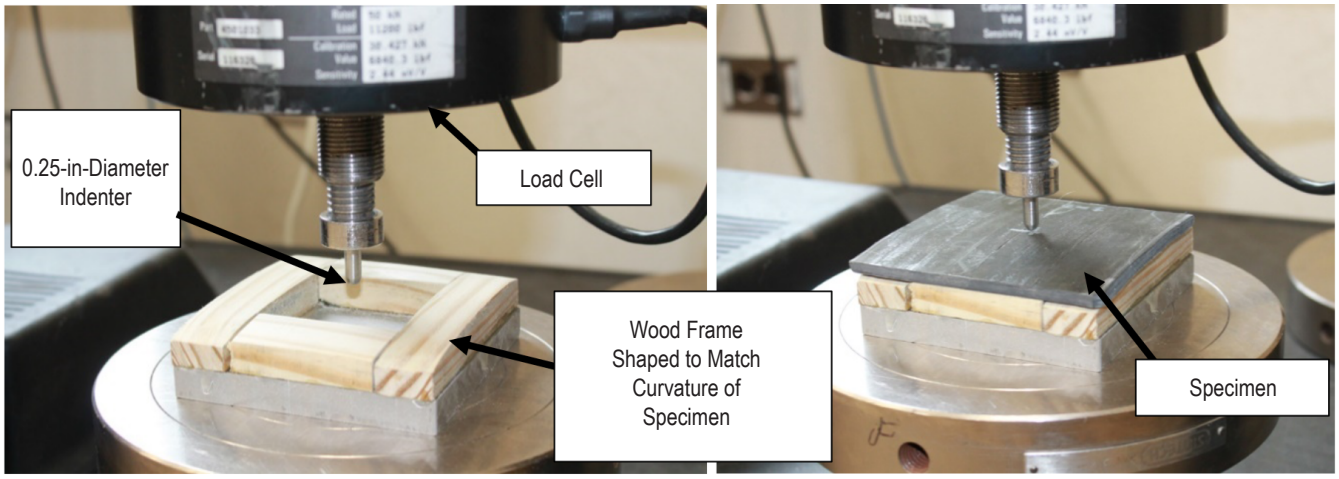

Figure 21. Static indentation test methodology.

6. RESULTS OF STATIC INDENTATION TESTING

An overlay of the load displacement data generated during the static indentation tests are shown in figure 22. Note that on some of the IM7 fiber specimens, the maximum load of 2,200 lb could not be reached. For these specimens a maximum load was reached and then the load began to rapidly drop.

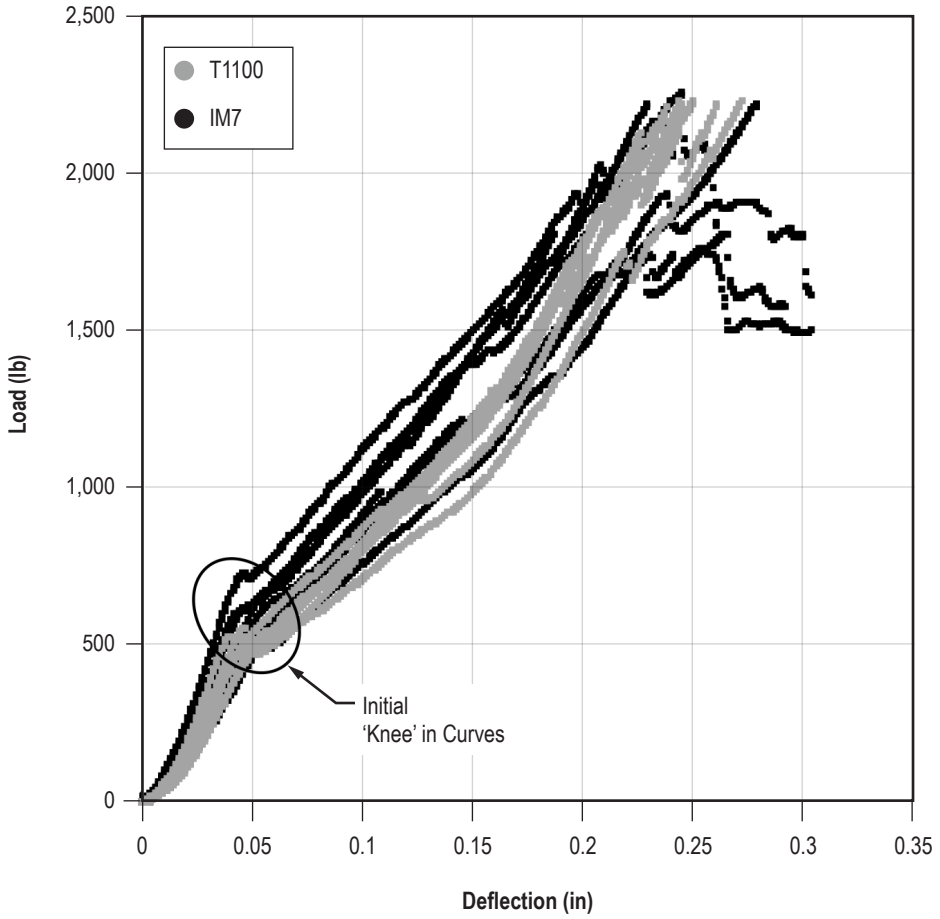

Figure 22. Overlay of load-deflection plots of the static indentation tests with both types of fibers.

In general, the so-called 'knee' indicated in figure 22, which occurred at ≈500 lb, had a slightly lower value (≈10%) in the curves of the T1100 fiber specimens than in the curves of the IM7 fiber specimens. In addition, the T1100 fiber specimens demonstrated some flexural stiffening, as noted by the upward curve of these data after the 'knee;' whereas the IM7 fiber specimen load-deflection behavior remained somewhat linear.

Examples of the visual damage produced by these tests are shown in figure 23. The IM7 fiber specimens are on the top row and the T1100 fiber specimens are on the bottom row. The top-right photograph is from an IM7 fiber specimen that did not reach the 2,200 lb of maximum load but experienced a maximum load of about 1,800 lb before the indenter began to penetrate through the specimen with no further increase in load. All of the IM7 fiber specimens exhibited the horizontal cracks seen on some of the drop-weight-impacted IM7 fiber specimens. A few of the T1100 fiber specimens also exhibited these horizontal surface cracks, but most did not. In general, these results were the same as the impact damage, where slightly more visual damage can be seen on the IM7 fiber specimens.

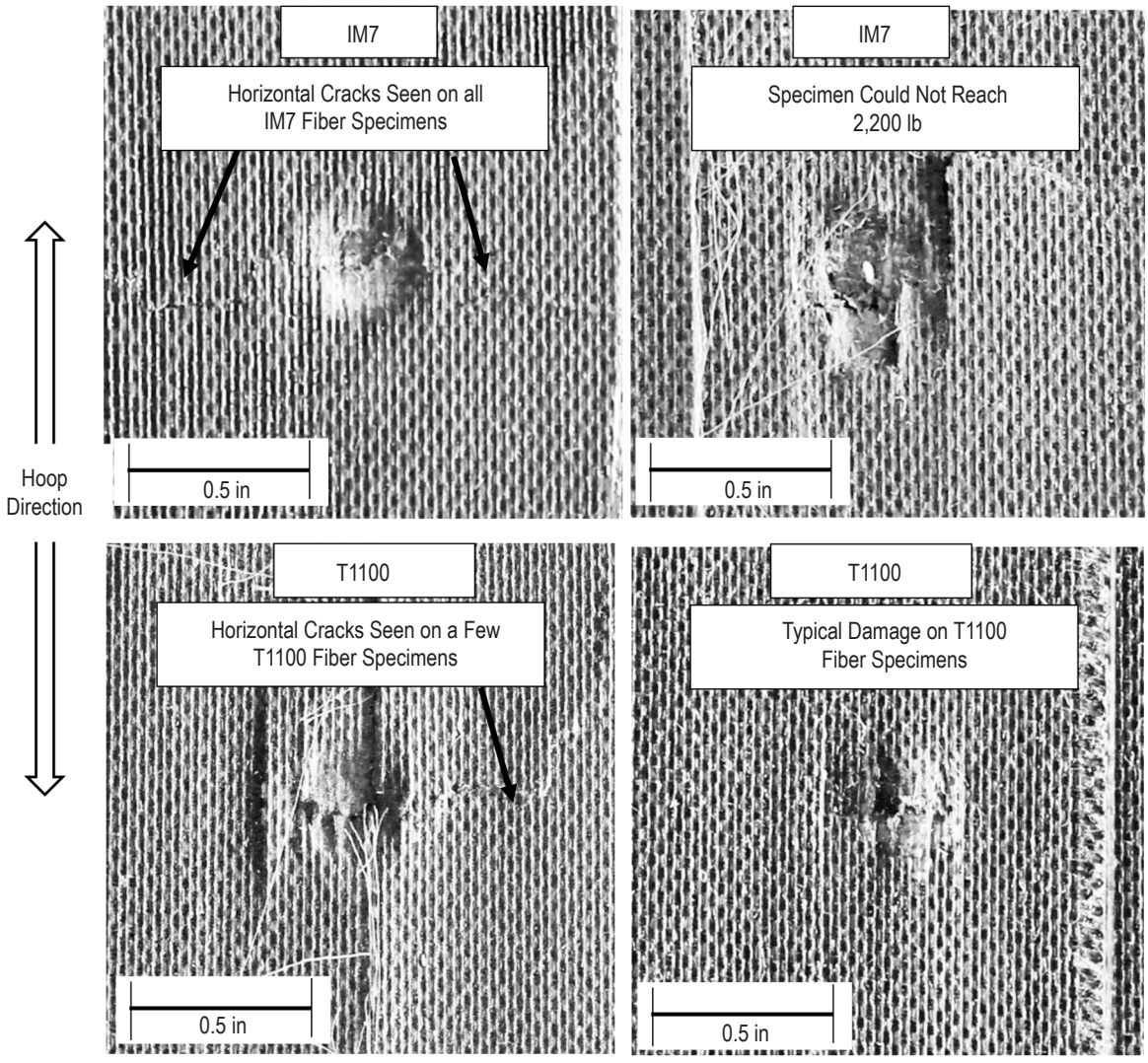

Figure 23. Damage caused by static indentation testing. IM7 fiber specimens top row, T1100 fiber specimens bottom row.

Thermography was performed on some of these specimens and typical results from inspecting from both the top and the bottom surfaces are shown in Figure 24. In general, all specimens exhibited the butterfly-shaped area of damage when examined from the back surface of the specimens. The internal damage was not as evident when examined from the front side of the specimen, with the T1100 fiber specimens showing slightly more damage when examined from the front. The thermography indications are delaminations within the specimen, which will not affect the burst strength of a pressure vessel. The fact that more delaminations are seen closer to the bottom of the specimen is typical of the conical shape of delamination damage in a laminated composite due to impact and will be seen in cross-sectioned specimens in the following section.

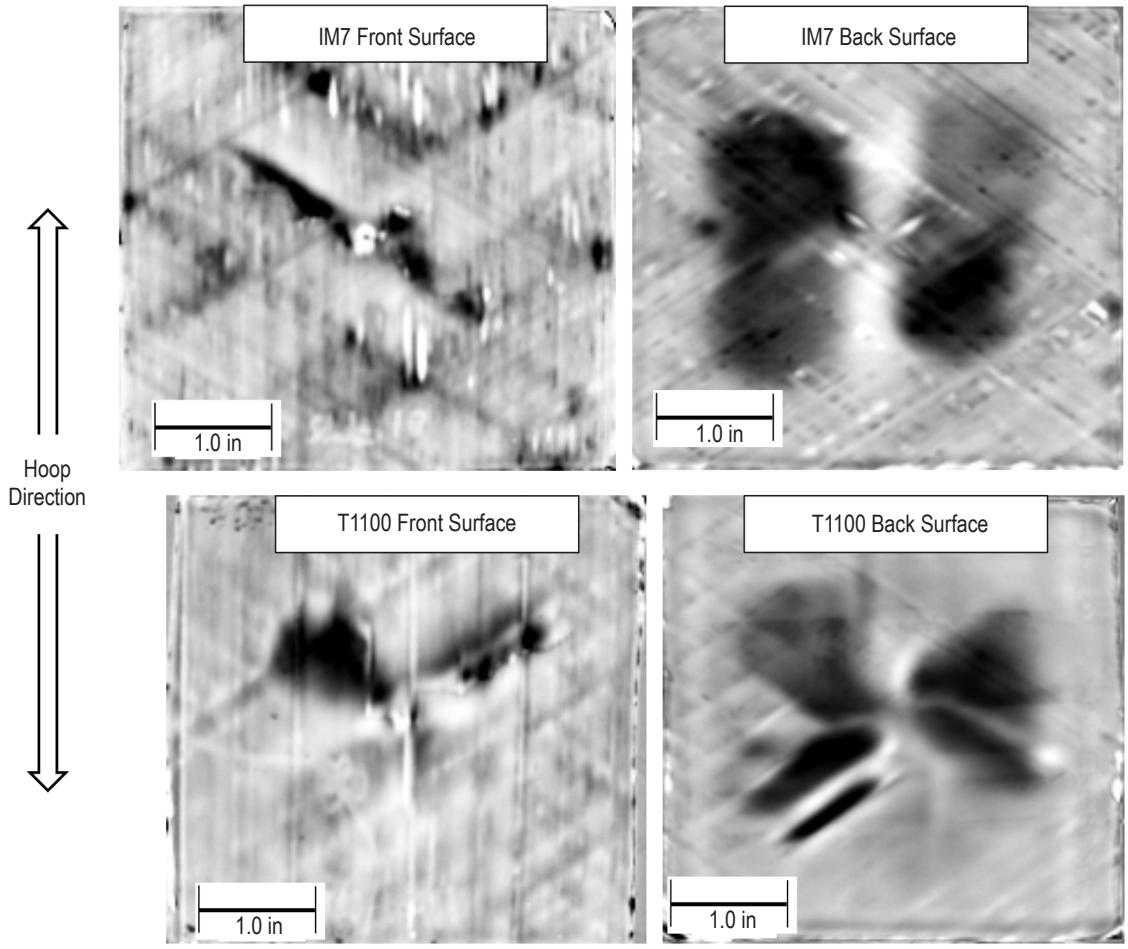

Figure 24. Thermography of damage caused by static indentation testing. IM7 fiber specimens top row, T1100 fiber specimens bottom row.

To obtain an overall view of the damage formed in each type of specimen, the specimens shown in figure 24 were sectioned through the damage zone in the hoop direction and examined using a standard camera (non-microscopy). To highlight the matrix cracking and delaminations, an ultraviolet (UV) penetrant was applied to the exposed cut surfaces and the excess wiped off. Photographs of the specimen were then taken under an ultraviolet light. The results are shown in figure 25.

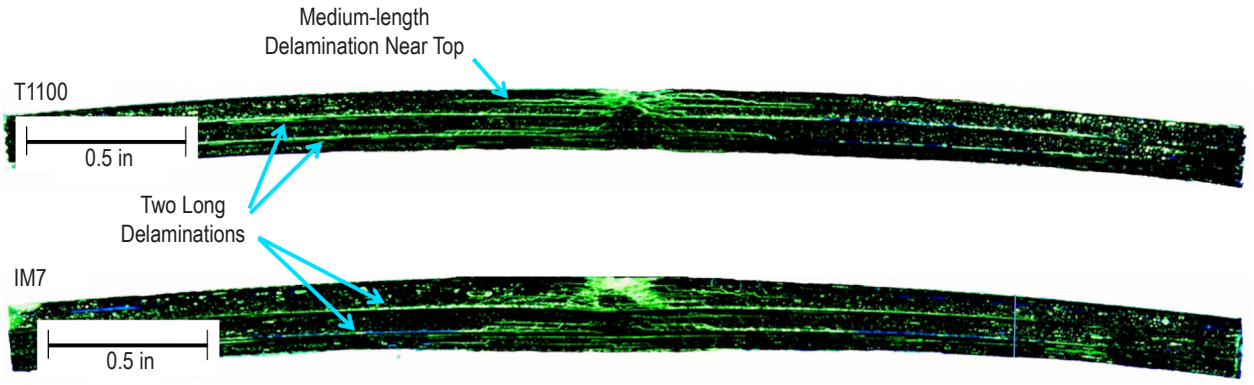

Figure 25. Ultraviolet photographs of cross sections of static indentation specimens seen in figure 24.

Both specimens showed two very long delaminations above the hoop plies, which probably comprised most of the thermography indication in figure 24. The T1100 specimen showed a medium-length delamination near the top, which is probably why these specimens showed more damage when flashed from the top surface.

A closer view of this medium-length delamination on the T1100 specimen and its comparison with the IM7 specimen is shown in figure 26, which was taken under white light magnification.

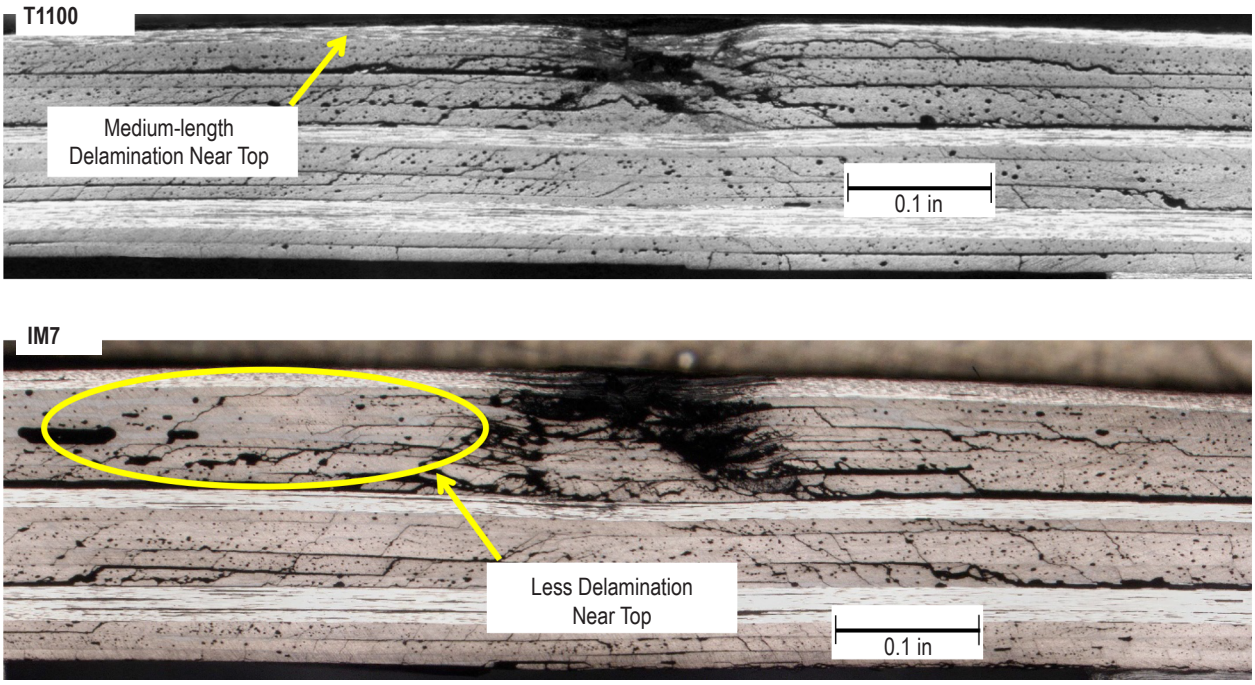

Figure 26. Cross sections of static indentation specimens seen in figures 24 and 25.

Since different sizing agents were used for each of the two types of fibers, perhaps the fiber/matrix bond is stronger on the IM7 specimens and more delaminations form within the T1100 specimens. This is somewhat a moot point as delaminations are not of concern; fiber breakage is the critical parameter that will affect burst-after-impact strength.

The sizing agent to be used in construction of the BOLE case may differ from those used in this study. Subscale damage tolerance testing on ring-burst specimens can determine if the sizing has any effect on the damage tolerance characteristics.

Since fiber breakage is the critical parameter being examined in this study, more specimens were sectioned through the damage zone and observed under magnification to look for fiber breakage. Examples of the damage in seven of each type of specimen using cross-sectional microscopy are shown in figure 27. The results are presented from least damage to most damage for a better side-by-side comparison. The IM7 fiber specimens are shown in the left column and the T1100 fiber specimens are shown in the right column. The maximum transverse load experienced by each specimen is indicated in the figure.

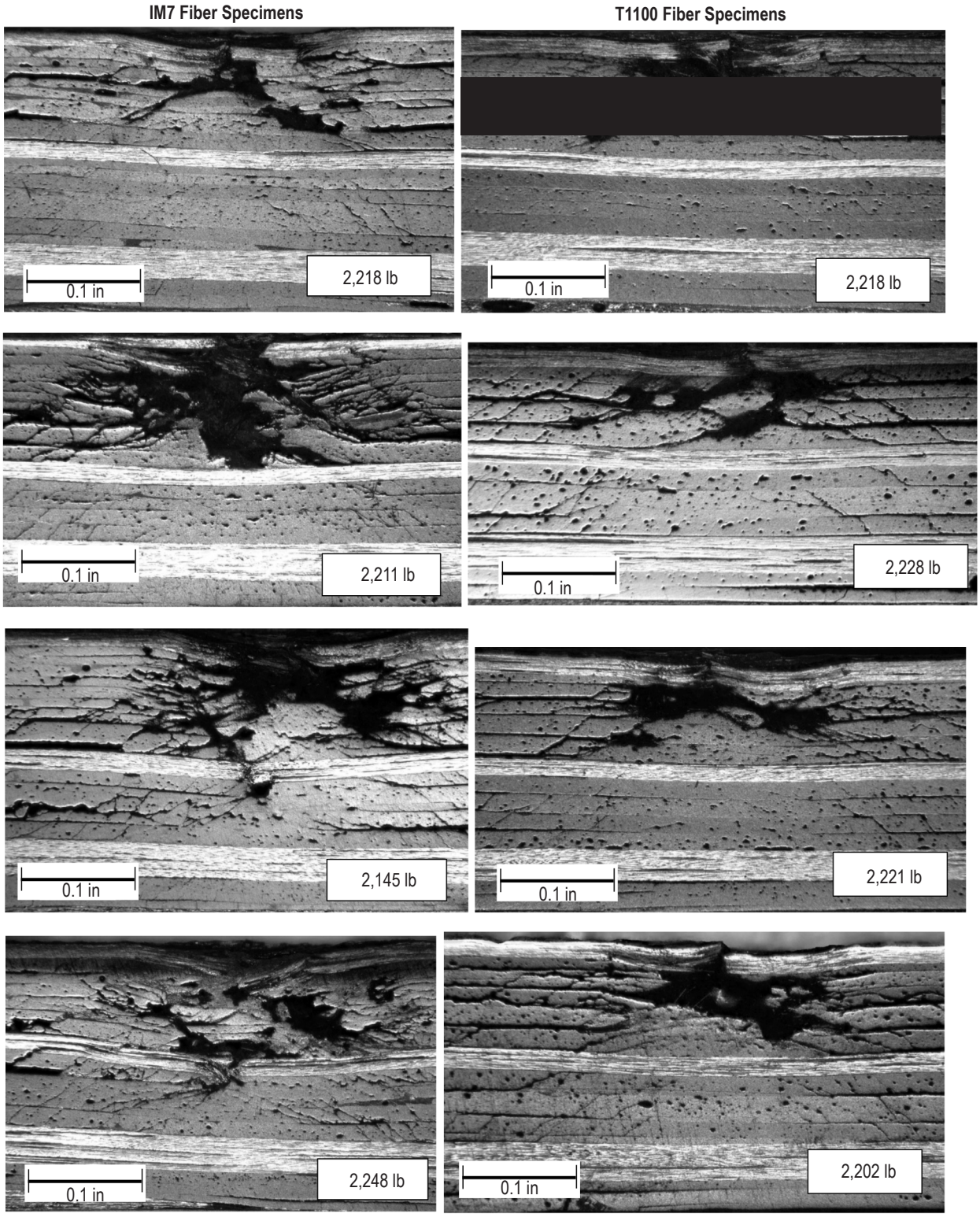

Figure 27. Cross sections of select static indentation specimens.

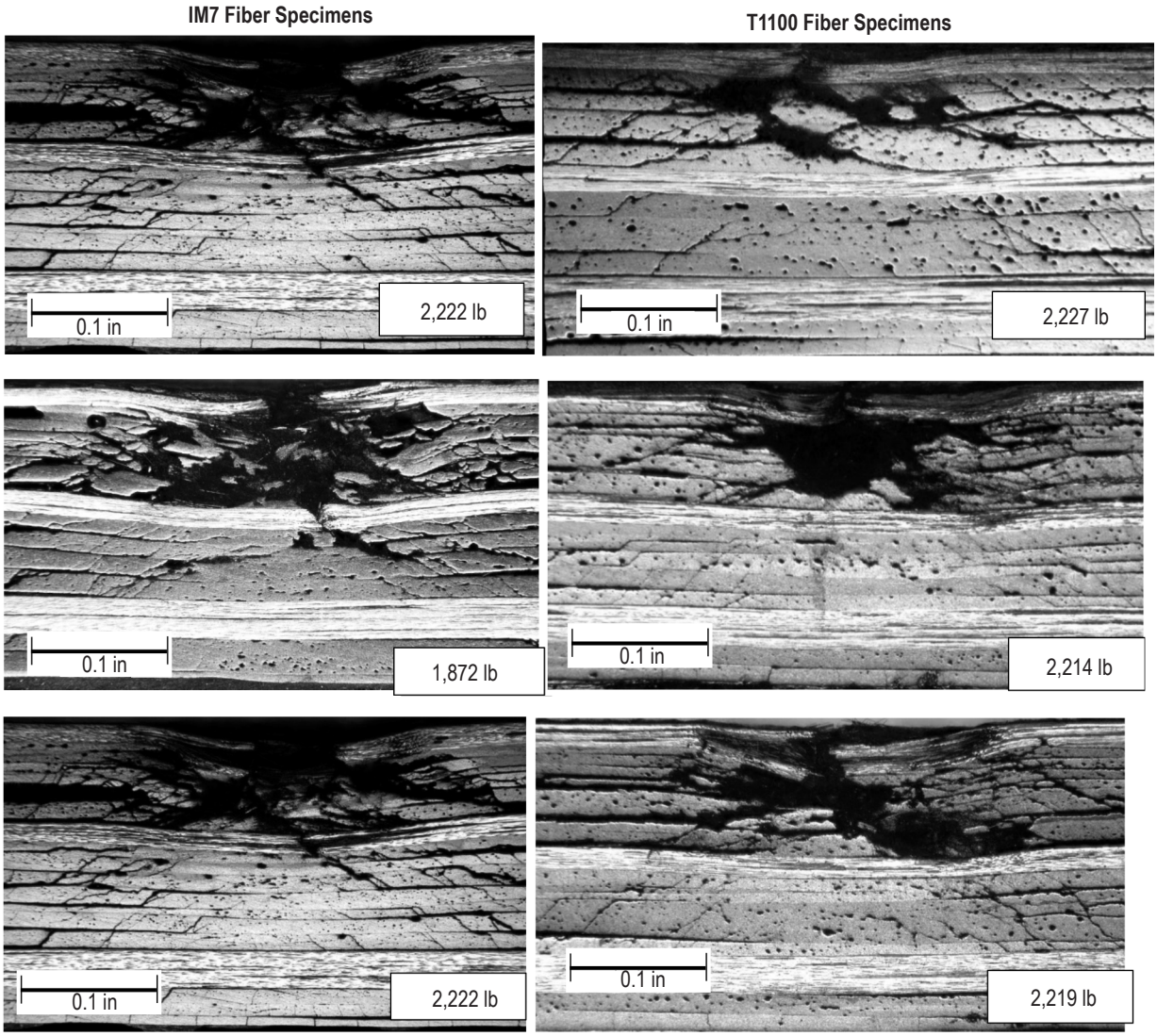

Figure 27. Cross sections of select static indentation specimens (Continued).

From these cross sections, the T1100 fiber specimens appear to be slightly more damage resistant with respect to fiber breakage than the IM7 specimens, except for the instances where the maximum load of 2,200 lb could not be reached in the IM7 specimens; in those cases, much more (as opposed to slightly more) fiber breakage is seen in the IM7 fiber specimens than in the T1100 fiber specimens.

As mentioned previously, the biggest difference in the load-deflection curves of the static indentation tests were at the first 'knee' in the curve. This 'knee' began at ≈600 lb for the IM7 fiber specimens and at ≈500 lb for the T1100 fiber specimens. A select number of tests were performed on specimens with both types of fiber and halted after the 'knee' was noted in order to determine what was causing this 'knee' (e.g., fiber breakage or delamination). Figure 28 shows sample load-deflection curves for a sample with each type of fiber.

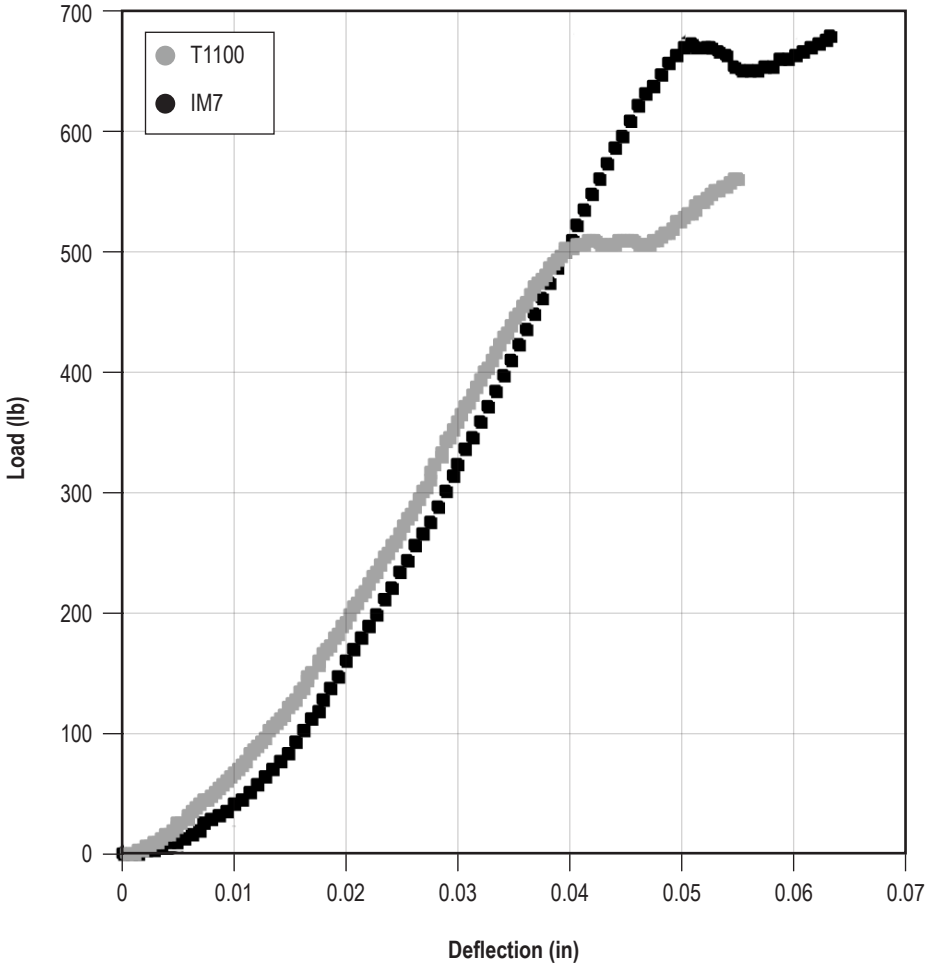

Figure 28. Load-deflection curves of two specimens with loading stopped after 'knee' in curve was noted.

Thermography images (from the back surface) were performed, and typical results are shown in Figure 29. From these images it appears that delaminations have begun at this stage of transverse loading.

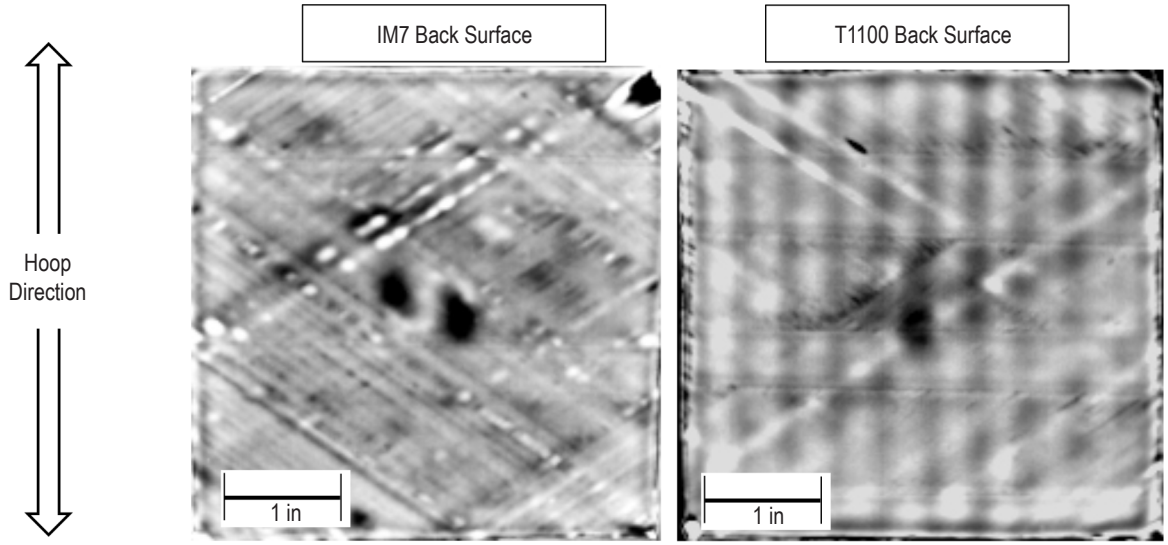

Figure 29. Thermography of damage caused by static indentation testing stopped after formation of 'knee' in load-deflection curve. IM7 fiber specimen left, T1100 fiber specimen right.

To get a full internal view of the damage after the formation of the 'knee,' some specimens were cross sectioned in the hoop direction through the loading point and observed under magnification. The results for one of each type of specimen is shown in figure 30.

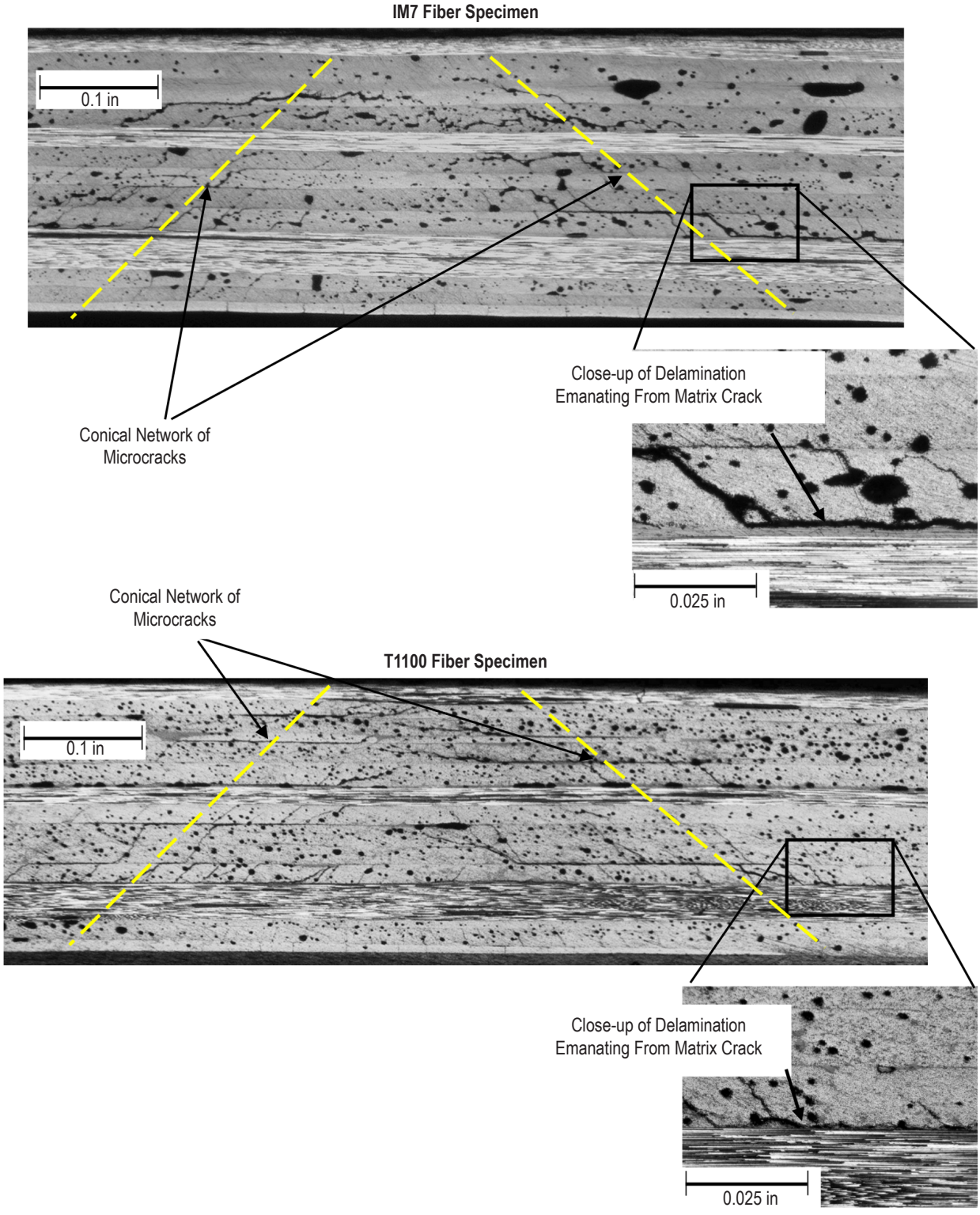

Figure 30. Cross sections of static indentation specimens stopped after 'knee' in load-deflection curve. IM7 top, T1100 bottom. Highlighted are closer views of delamination emanating from matrix crack at the hoop/helical interface.

At this point no fiber damage can be seen, but the damage consists of the typical conical network of matrix cracks and delaminations. To determine if the 'knee' corresponds to the onset of the matrix cracks, delaminations, or both, a few specimens were loaded to about 100 lb below where the 'knee' was forming and examined for the internal damage. A cross section of one of these specimens is shown in figure 31 and it can be seen that at this point, the matrix cracks have formed, but the delaminations have not.

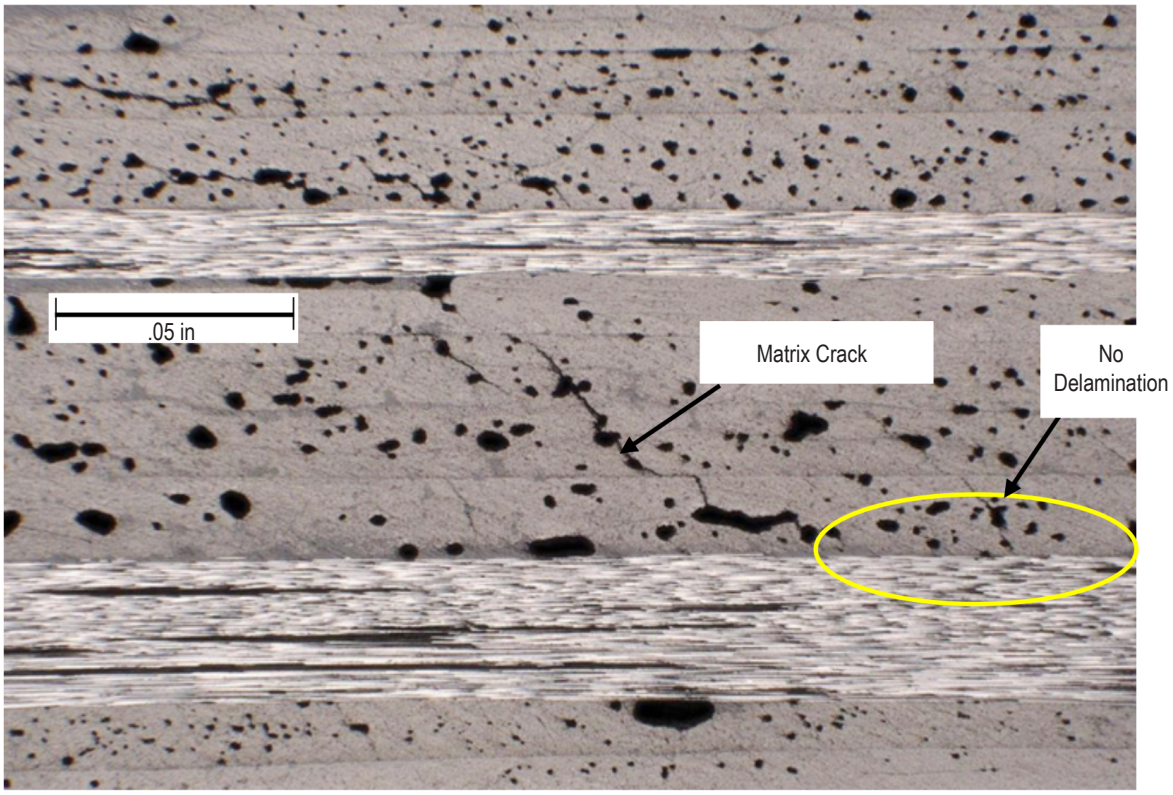

Figure 31. Cross section of static indentation specimen stopped before 'knee' in load-deflection curve.

Thus the 'knee' seen in the load-deflection curves corresponds to the onset of delamination in the specimens. Since the resin is the same, the only difference may be in how well the resin and fiber adhere to one another. This can be due to what type of sizing agent is used, if any. Since different sizing agents were used for the two types of fibers, this is the most likely explanation. In most applications, the best fiber/matrix bond that can be achieved is desired. However, for tension-driven structure such as pressure vessels, this may not be true, as a weaker fiber/matrix interface will cause more impact energy to go into delamination damage rather than fiber breakage—and it has already been established that delaminations are benign to burst strength of a rocket motor case.

To test the hypothesis that the T1100 fiber specimens were delaminating before the IM7 fiber specimens, a series of short beam shear (SBS) tests were carried out. Specimens 1.2 × 0.4 in were excised from each of the two cylinders and tested per American Society for Testing and Materials (ASTM) D2344, Standard Test Method for Short-Beam Strength of Polymer Matrix Composite Materials and their laminates. This test is basically a miniature 3-point bend test. A photograph of this test method is shown in figure 32.

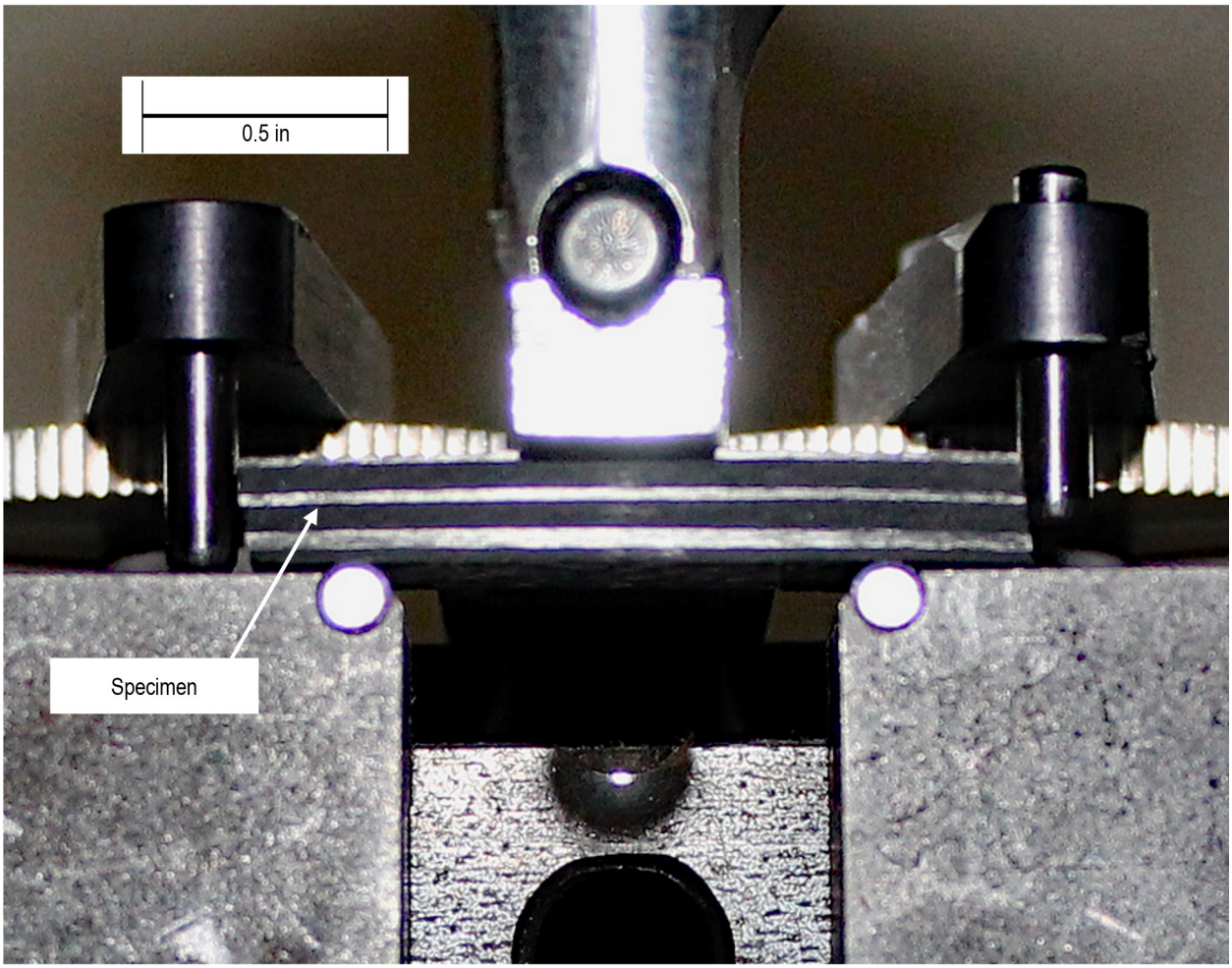

Figure 32. Setup of SBS test.

This test causes the specimen to fail by Mode II delamination, which is the same mode of delamination failure due to an impact on laminates. Since the resin is the same and the fibers are not failing, any differences may be attributed to how well the resin bonds to the fiber (i.e., due to the sizing agent).

Figure 33 shows examples of failed SBS specimens; it can be seen that delamination is the failure mode.

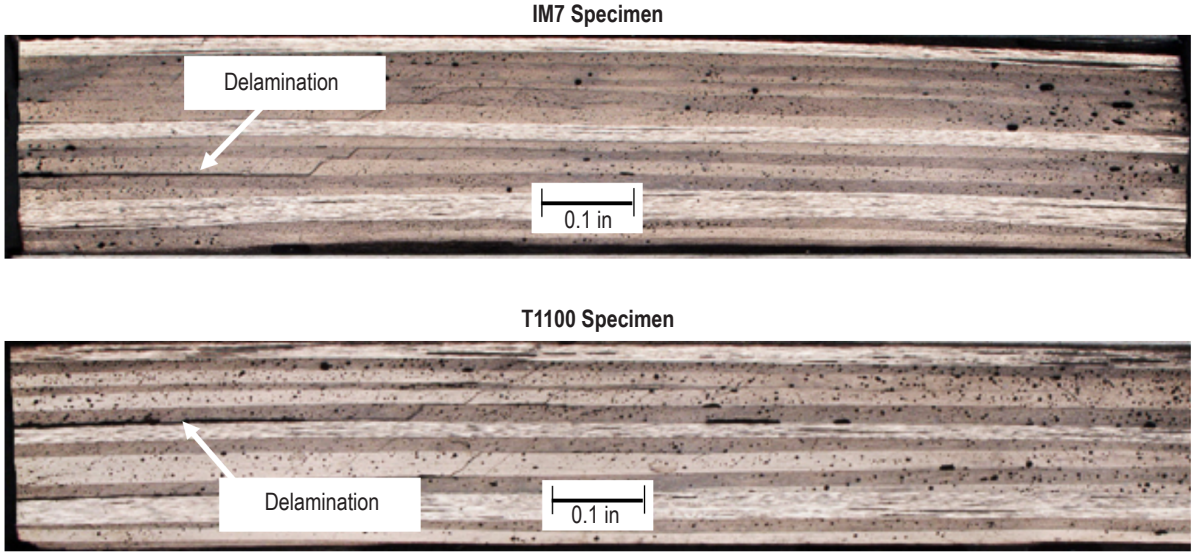

Figure 33. Failed SBS test specimens.

Table 5 summarizes the results of the SBS tests. The reported failure stress is the maximum load attained during the test divided by the specimen thickness and width.

Table 5. Results of SBS tests.

Specimen #	Failure Stress (psi)
T1100-1	5588
T1100-2	6116
T1100-3	5309
T1100-4	5653
T1100-5	6310
T1100-6	5373
T1100-7	5498
T1100-8	5623
T1100-9	5373
T1100-10	5372
T1100 Average	5618±340

Specimen #	Failure Stress (psi)
IM7-1	6201
IM7-2	6540
IM7-2	5794
IM7-2	6336
IM7-2	6603
IM7-2	5797
IM7-2	6046
IM7-2	6231
IM7-2	5839
IM7-2	6029
IM7 Average	6142±293

The average failure stress of the T1100 fiber specimens is 8.5% lower than the IM7 fiber specimens, which is about the same magnitude less as the load of the 'knees' seen in the static indentation tests.

7. CONCLUSIONS

From the results presented in this study, the T1100 fiber appears to be slightly more damage resistant when manufactured via wet winding. This is not surprising, given that the T1100 fiber has a higher elongation to failure and should be able to absorb more energy before fracture. In addition, the T1100 fiber samples tend to show slightly more delaminations, which helps protect the fiber by allowing energy to be dissipated by this mechanism rather than fiber breakage. This is probably due to the different sizing agents used. Thus, the results of the damage tolerance study of rocket motor cases made from IM7 carbon fiber[3] can be applied to rocket motor cases made of T1100 carbon fiber without the need for further full-scale damage tolerance testing.

REFERENCES

1. Nettles, A.T.: "Impact Damage Resistance of the Launch Abort System Filament-Wound Rocket Motor Case," NASA/TM—2017–219845, NASA Marshall Space Flight Center, Huntsville, AL, 60 pp., December 2017.
2. Nettles, A.T.: "A Brief Overview of the Effects of Impact Damage to Rocket Motor Cases," NASA/TM—2020–5007139, NASA Marshall Space Flight Center, Huntsville, AL, 38pp., September 2020.
3. Dalton, T.: "Advanced Booster EDRR Final Report, Volume 6: Composite Case Reliability Assurance System (CCRAS) Overall Project Summary," Technical Report TR033091-06, Orbital ATK, Dulles, VA, 2 pp., April 2015.
4. Nettles, A.T. and Douglas, M.J.: "A Comparison of Quasi-Static Indentation to Low-Velocity Impact," NASA/TP—2000–210481, NASA Marshall Space Flight Center, Huntsville, AL, 98 pp., August 2000.

National Aeronautics and
Space Administration
IS02
George C. Marshall Space Flight Center
Huntsville, Alabama 35812